Published OnlineFirst July 25, 2012; DOI:10.1158/0008-5472.CAN-12-0271

Cancer Research

MicroRNAs Regulate Tumor Angiogenesis Modulated by Endothelial Progenitor Cells

Prue N. Plummer, Ruth Freeman, Ryan J. Taft, et al.

Cancer Res 2013;73:341-352. Published OnlineFirst July 25, 2012.

Published OnlineFirst July 25, 2012; DOI:10.1158/0008-5472.CAN-12-0271

MicroRNAs Regulate Tumor Angiogenesis Modulated by Endothelial Progenitor Cells

Prue N. Plummer[1], Ruth Freeman[1], Ryan J. Taft[2], Jelena Vider[1], Michael Sax[1], Brittany A. Umer[1], Dingcheng Gao[7], Christopher Johns[8], John S. Mattick[2], Stephen D. Wilton[4], Vito Ferro[3], Nigel A.J. McMillan[1], Alexander Swarbrick[5,6], Vivek Mittal[7], and Albert S. Mellick[1]

Abstract

Bone marrow–derived endothelial progenitor cells (EPC) contribute to the angiogenesis-dependent growth of tumors in mice and humans. EPCs regulate the angiogenic switch via paracrine secretion of proangiogenic growth factors and by direct luminal incorporation into sprouting nascent vessels. miRNAs have emerged as key regulators of several cellular processes including angiogenesis; however, whether miRNAs contribute to bone marrow–mediated angiogenesis has remained unknown. Here, we show that genetic ablation of miRNA-processing enzyme Dicer, specifically in the bone marrow, decreased the number of circulating EPCs, resulting in angiogenesis suppression and impaired tumor growth. Furthermore, genome-wide deep sequencing of small RNAs revealed tumor EPC-intrinsic miRNAs including miR-10b and miR-196b, which have been previously identified as key regulators of HOX signaling and adult stem cell differentiation. Notably, we found that both miR-10b and miR-196b are responsive to vascular endothelial growth factor stimulation and show elevated expression in human high-grade breast tumor vasculature. Strikingly, targeting miR-10b and miR-196b led to significant defects in angiogenesis-mediated tumor growth in mice. Targeting these miRNAs may constitute a novel strategy for inhibiting tumor angiogenesis. *Cancer Res; 73(1); 341–52. ©2012 AACR.*

Introduction

For a solid tumor to grow and spread it must recruit blood vessels in a process referred to as the angiogenic switch (1). Bone marrow–derived endothelial progenitor cells (EPC) are important mediators of the angiogenic switch through the production of paracrine factors and by directly incorporating into the lumen of tumor neovasculature. Suppression of EPCs leads to a delayed angiogenic switch, which is associated with impaired tumor growth and spread (2–4). Tumor EPCs are phenotypically distinct from tumor vasculature, and other bone marrow–derived cells in the tumor microenvironment. Therefore, targeting EPC-intrinsic factors provides a therapeutic approach, likely to be devoid of undesired side effects associated with current antiangiogenic therapies (4–7). However, mechanisms of EPC-mediated tumor angiogenesis need further investigation.

miRNAs (miRNA/miR) are small noncoding RNAs (18–23 bp in size) generated by the consecutive activity of 2 RNAseIII enzymes, Drosha and Dicer (8). They regulate gene activity by sequence-specific binding to mRNA, triggering either translational repression or RNA degradation. It has been predicted that mammalian miRNAs regulate approx. 30% of all protein-coding genes (9). miRNAs have emerged as key regulators of several cellular processes, including angiogenesis (10). A major indicator that miRNAs may contribute to angiogenesis came from the observation that suppression of Dicer and Drosha *in vitro* resulted in impaired angiogenesis (11–13). It has also been shown that tissue-specific inactivation of Dicer leads to impaired vascular development in the embryo (14). However, miRNAs have not been directly implicated in EPC-mediated tumor angiogenesis *in vivo*.

Previously, we have shown that the proximal promoter of the inhibitor of DNA binding 1 (Id1), in a retroviral context, can be used to genetically modify and deliver transgenes to EPCs *in vivo* (4). We also showed that Id1-marked EPCs could be tracked from the bone marrow compartment to the tumor bed, where they were eventually incorporated into the tumor vasculature. Using a similar strategy, we delivered Cre-recombinase to specifically excise floxed Dicer, the key miRNA-processing

Authors' Affiliations: [1]School of Medical Science, Griffith University, Parklands Dr, Gold Coast; [2]Genomics & Computational Biology, Institute for Molecular Bioscience, University of Queensland; [3]School of Chemistry and Molecular Biosciences, University of Queensland, St Lucia, Queensland; [4]Experimental Molecular Medicine Group, Centre for Neuromuscular and Neurological Disorders, University of Western Australia, Nedlands, Western Australia; [5]Garvan Institute of Medical Research, Darlinghurst, Sydney; [6]St Vincent's Clinical School, Faculty of Medicine, University of New South Wales, New South Wales, Australia; [7]Department of Cardiothoracic Surgery and Neuberger Berman Lung Cancer Center, Weill Cornell Medical College, Cornell University, New York; and [8]Microarray Shared Resource Facility, Cold Spring Harbor Laboratories, Cold Spring Harbor, New York

Note: Supplementary data for this article are available at Cancer Research Online (http://cancerres.aacrjournals.org/).

Corresponding Authors: Albert S. Mellick, School of Medical Science, Griffith University, Parklands Dr, Gold Coast, QLD 4215, Australia. Phone: 61-7-55-52-72-73; Fax: 61-7-55-52-89-08; E-mail: a.mellick@griffith.edu.au; and Vivek Mittal, Weill Cornell Medical College, Cornell University, 1300 York Avenue, New York, NY 10021. E-mail: vim2010@med.cornell.edu

doi: 10.1158/0008-5472.CAN-12-0271

Published OnlineFirst July 25, 2012; DOI:10.1158/0008-5472.CAN-12-0271

enzyme in EPCs, which resulted in global miRNA loss and impaired EPC-mediated tumor angiogenesis. To identify candidate miRNAs, we conducted a genome-wide small RNA sequencing of tumor EPCs, revealing a miRNA profile that was more similar to vasculature from normal tissues and tumors, than either bone marrow–derived myeloid and/or lineage-depleted (Lin^-) cells. Notably, we identified several miRNAs, in particular miR-10b and miR-196b (15–17), which were upregulated in tumor EPCs and tumor vasculature, compared with EPCs from wild-type animals and normal vasculature, respectively. We also showed that miR-10b and miR-196b are regulated by tumor-conditioned media and VEGF in endothelial cells, and that suppression of both miRNAs led to significant endothelial cell defects *in vitro*, as well as EPC-mediated impaired tumor growth *in vivo*. Taken together, these results underscore the importance of miRNAs in EPC-mediated tumor angiogenesis and provide novel targets for future antiangiogenic strategies.

Materials and Methods

Mice

The method for obtaining transgenic mice with the floxed Dicer allele (18) and Cre-recombinase, as well as the Id1 reporter mice (19) is outlined in the Supplementary Methods. Female C57BL/6 mice, BALB/c mice, and immunocompromised BALB/c nu/nu (nude) mice were obtained from the Animal Resources Centre (Canning Vale, Western Australia). All procedures involving mice were conducted in accordance with protocols reviewed and approved by institutional animal care, and ethics committees.

Human biopsies

Formalin-fixed breast cancer biopsies cryopreserved in OCT were provided by the Breast Cancer Tissue Bank (www.abctb.org.au). Biopsies were collected by Westmead Hospital, Australia, under protocols reviewed and approved by the institutional human ethics committees. In this study, biopsies representing the most common type of invasive breast cancer, infiltrating ductal carcinoma (IDC), and the most common type of noninvasive breast cancer ductal carcinoma *in situ* (DCIS; ref. 20) were prepared as 10-μm-thick transverse sections before *in situ* hybridization (ISH) analysis.

Cell lines and cell culture conditions

Murine Lewis lung carcinoma cells (LLC)/D12 were obtained from the American Type Culture Collection (ATCC) and were provided by Eisenbach (Wiesman Institute of Science, Rehovot, Israel), and maintained in RPMI and 10% fetal calf serum (FCS; Invitrogen). An LLC cell line expressing the monomeric form of the red fluorescent protein mCherry (21) was created through the stable transduction of a retroviral construct containing mCherry, driven by a 500 bp region of the murine phosphoglycerate kinase promoter (3). LLC–mCherry clones were selected for *in vivo* studies based on similarity in growth and pathology to the parental line. The murine 4T1 and human MDA-MB-231 mammary carcinoma cell lines were obtained from the ATCC and maintained in Dulbecco's Modified Eagle's Medium (DMEM) with 10% FCS.

Human embryonic kidney (HEK) 293T cells were obtained from ATCC and grown in DMEM, with 10% FCS and sodium pyruvate (1 mmol/L). ROSA26-Lox-Stop-Lox-*β-lactomase* (LacZ) 3T3 fibroblasts containing *Lac*Z, under the control of a *floxed* transcriptional termination sequence (obtained from the Lowe Lab; ref. 22), were maintained in DMEM and 10% FCS. Human umbilical vein endothelial cells were obtained from ATCC, grown on 0.1% gelatin (Sigma-Aldrich), and maintained in EGM-2MV BulletKit Media (Lonza), supplemented with VEGF and fibroblast growth factor. Murine endothelial cells were provided by J. Cook-Mills (University of Cincinnati, Cincinnati, OH; ref. 23) and maintained in DMEM with 10% FCS. Cell authentication was conducted at ATCC by short tandem repeat profiling, cell morphology monitoring, karyotyping, and the ATCC cytochrome *c* oxidase. All cultures obtained were resuscitated from stocks frozen at low passage within 6 months of receipt.

Bone marrow transplant and tumor growth studies

Bone marrow transplant (BMT) was conducted using previously published protocols (ref. 4; see also Supplementary Fig. S1A). Once fully reconstituted (8 weeks), BMT mice were then treated with 4-hydroxytamoxifen (4-OHT) in sesame oil (200 μg per animal; Sigma Aldrich), by intraperitoneal injection every 2 days: beginning 4 days before tumor implantation (see also Supplementary Fig. S1A). For tumor growth studies, animals were inoculated with: (i) 5×10^6 LLC cells (intradermally in C57BL/6 mice); (ii) 5×10^4 4T1 breast cancer cells (orthotopically in the mammary fat pad of BALB/c mice); or (iii) 1×10^6 MDA-MB-231 cells (orthotopically in the mammary fat pad of nude mice). For all experiments, tumor volume was measured using standard methods (4, 24).

Generation of Cre-recombinase lentiviral constructs

To deliver Cre-ERT2, under the control of the Id1 proximal promoter (Id1pr/p), Cre-ERT2 was inserted into a *Not*I site upstream of GFP in the lentiviral (LV) pWPT-Id1pr/p-GFP construct, as previously described (4). An internal ribosome entry site (IRES) was inserted between GFP and Cre-ERT2 to create LV-Id1pr/p-GFP-*IRES*-Cre^{ERT2} (Id1pr/p-Cre^{ERT2}). A constitutive Cre-ERT2 expressing control construct was created by replacing the Id1pr/p element with an 800 bp region of the elongation factor (EF) 1α1 promoter to generate LV-pWPT-EF_{long}-GFP-*IRES*-Cre^{ERT2} (EF_{long}-Cre^{ERT2}). In this study, LV production was conducted using a three vector packaging system, with the HIV gag-pol-encoding psPAX.2 (pMDLg/pRRE and REV) and pMD2.G (VSVG; Addgene), cotransfected into the 293T packaging cell line (25). Viral titer was determined by p24 ELISA (Perkin-Elmer), and/or fluorescence-activated cell sorting (FACS) analysis of GFP signal in LV-pWPT-GFP infected 293T cells. Finally, the "Cre-ERT2 activity" of infected cells was assessed by (i) gene activation, following infection of ROSA26-Stop-Lox-Stop-LacZ 3T3 fibroblasts; and (ii) self-inactivation of GFP, following 4-OHT induction of LV Cre-recombinase transduced 293T cells. LV transduction of bone marrow and analysis of transduction efficiency (integration

Published OnlineFirst July 25, 2012; DOI:10.1158/0008-5472.CAN-12-0271

events/genome) before (and after) BMT were conducted as described (4).

Fluorescent immunohistochemical microscopic analysis of tissues

Unless otherwise stated, all tissues were stained with Alexa Fluor (Invitrogen) or phycoerythrin (PE) conjugated primary antibodies and with the nuclear counter stain, 4′,6-diamidino-2-phenylindole (DAPI). Rat antimouse primary antibodies: CD31/PECAM-1 (clone MEC13.3), VE-cadherin/CD144 (clone 11D4.1), CD11b (clone M1/70), VEGFR2/Flk1 (clone avas12α1), and PE-conjugated c-kit/CD117 (clone 2B8), were obtained from BD Pharmingen. Primary mouse antihuman monoclonal antibody CD31 (clone WM59) was obtained from BD Biosciences. Polyclonal rabbit anti-CRE recombinase (ab40011) from Abcam, polyclonal goat anti-HOXD10 (catalog no. 33005) from Santa Cruz; and rabbit anti-Dicer polyclonal antibody (kindly provided by G. Hannon, CSHL, NY) were detected with Alexa Fluor conjugated anti-rabbit (Invitrogen)/or anti-goat (Santa Cruz) secondary antibody, using established protocols (2–4). GFP and mCherry were detected by their own fluorescence signal (4, 19, 21). Images were obtained using the Zeiss Z1 fluorescent microscope (Software Axiovision Version 4.8; Carl Zeiss) with a resolution of 0.275 to 0.35 μm, as described (2–4).

Locked nucleic acid *in situ* hybridization analysis of tissues

Cell-specific small RNAs were detected by fluorescence microscopy using modification of previously published methods (26, 27). After OCT removal, the slides were subjected to another round of fixation in 4% PFA (5–10 minutes). The tissues were blocked (50 × Denhardt's, 10 mg/mL Yeast tRNA, 10 mg/mL Salmon Sperm DNA, formamide, 20 × SSC pH7, 50°C, 10–20 minutes). To detect miRNAs, 2 pmol of 5′-Digoxigenin (DIG) labeled LNA RNA oligonucleotide probe (miRCURY Exiqon) was added and slides were incubated: 30 minutes for adherent cells or 80 minutes for tissue sections (50°C). All experiments were conducted with negative (scrambled: 5′-DIGN/GTGTAACACGTCTATACGCCA-3′) and positive (U6: 5′-DIGN/CACGAATTTGCGTGTCATCCTT-3′) control probes. The following locked nucleic acid (LNA) probes were used in this study: miR-10b (5′-DIGN/CACAAATTCGGTTCTACAGGTA-3′), miR-196b (5′-DIGN/CCCAACAACAGGAAACTACCTA-3′), miR-451 (5′-DIGN/AACTCAGTAATGGTAAGGTTT-3′), miR-132 (5′-DIGN/CGACCATGGCTGTAGACTGTTA-3′), miR-151-3p (5′-DIGN/CCTCAAGGAGCCTCAGTCTAG-3′), and miR-152 (5′-DIGN/CCAAGTTCTGTCATGCACTGA-3′). The slides were then washed with: (i) 0.1 × SSC, 10 minutes, 54°C three times; (ii) 2 × SSC, 5 minutes, room temperature once; and (iii) TN buffer (0.1 mol/L Tris-HCL with 0.15 mol/L NaCl) pH 7.5, 3 minutes, room temperature 3 times. The slides were then blocked, 2 hours room temperature with blocking buffer (0.1 mol/L Tris-HCl, pH 7, 0.15 mol/L NaCl, 0.3% TritonX-100, 10% FCS, 0.5% blocking reagent; Roche Applied Science). To detect DIG-labeled hybridized probe and cell-specific antigens, anti-DIG-fluorescein isothiocyanate (FITC) or anti-DIG-rhodamine (RHOD, in the case where FITC may overlap with GFP signal) conjugated, Fab Antibody Fragments (Roche Applied Science), and Alexa Fluor (Invitrogen)-conjugated primary antibodies were added to the blocking buffer (1:400) and incubated for adhered cells (2 hours, room temperature) and for tissue slides (overnight, 4°C). To validate the cytoplasmic compartmentalization of identified miRNAs, fluorescence detection by TRITC-conjugated phalloidin (#R415; Invitrogen), which selectively binds to F-actin was conducted (0.1 U/slide, overnight). After washing in TN buffer, supplemented with Tritron X-100 (1%), the tissue slides were stained with DAPI.

Isolation of mouse cells by FACS

FACS was used to analyze and isolate cell populations. Single-cell suspensions were obtained from bone marrow and PB, as described earlier, whereas fresh tumor and lung tissues were collagenase treated (Collagenase H&D; Roche Diagnostics, 37°C, 40 minutes). In each instance, single-cell suspensions were filtered (70 μm), preblocked with F_c block CD16/CD32 (BD Pharmingen), and incubated with primary Alexa Fluor conjugated monoclonal antibodies as described earlier. A rat monoclonal antimouse TER-119 (clone TER-119) antibody (BD Biosciences) was used as an erythroid marker (2–4). FACS was done with isotype, fluorescence-minus-one, and unstained controls for determining appropriate gates, voltages, and compensation (28), using the LSRII flow cytometer. Multivariate FACS analysis was done using FACS Diva software (BD Biosciences). Cells were stained and sorted into PBS, supplemented with 1% FCS, using the BD FACS Aria flow cytometer (BD Biosciences). mCherry LLC tumor cells, labeled with mCherry, were excluded from the host-derived vasculature, using the MoFlow (Beckman Coulter) high-speed cell sorter, with the Sapphire laser (561 nm Excitation; Coherent Inc.).

Small RNA analysis of FACS isolated mouse cells

Total RNA was obtained (TRIzol; Invitrogen), and salts were removed using the Amicon-Ultra 0.5 mL 3K columns (Millipore). RNA quality was assessed using the Nanodrop1000 (ThermoScientific) before analysis. Library preparation and sequencing was conducted by R. King (GeneWorks), using the Illumina alternative v1.5 protocol for small RNA sequencing on the Illumina Genome Analyzer (Illumina). Two '*Spike-in*' 5′-P and 3′-OH RNA oligonucleotides at 1 pmol/10 μg were used as internal normalisation controls: Spike02 (5′-P-AGUAACUCUAGCGGCUUAGUC-OH-3′) and Spike06 (5′-P-AUACGUCGACACGGUUCA-OH-3′; ref. 29).

Bioinformatic analysis was conducted on a high performance computing station (University of Queensland, St. Lucia, Queensland, Australia) that houses a local mirror of the UCSC Genome Browser20 (9), the Galaxy toolset (30), and a suite of publicly available and in-house programs. Library adaptors were removed using the FASTX-toolkit (http://hannonlab.cshl.edu/fastx_toolkit/). Sequences were mapped using Bowtie (31) and were required to map uniquely to the genome without mismatches. miRNA expression was computed using an in-house Galaxy pipeline that takes all small RNA sequences that map to miRBase Release 16 pre-miRNA and mature miRNA annotations (32). Relative expression differences were

Published OnlineFirst July 25, 2012; DOI:10.1158/0008-5472.CAN-12-0271

calculated for each feature using the spike control normalized values. Those sequences that showed less than 300 normalized reads were excluded from further analysis.

To validate the representation of miRNAs identified in each library, real-time quantitative reverse transcriptase PCR was conducted using miScript SYBR Green Kit (Qiagen). Amplification products were detected using the iCycler iQ (Bio-Rad). Relative-fold differences in expression were determined using comparative analysis of mean control and test cycle threshold ($\Delta\Delta C_T$) at linearity with respect to 1 of 2 internal reference small RNAs: U5a or U6 (Qiagen; ΔC_T; ref. 33).

Results

Conditional ablation of Dicer in bone marrow EPCs results in angiogenesis inhibition and impaired tumor growth

To determine whether miRNA biogenesis is required for bone marrow–mediated tumor growth and angiogenesis, total bone marrow from the Dicer$^{flox/flox}$/Cre$^{ERT2/-}$ mice was transplanted into irradiated syngeneic C57BL/6 wild-type recipient mice (Supplementary Fig. S1A). Following 8 weeks of stable bone marrow engraftment, administration of 4-OHT to Dicer$^{flox/flox}$/Cre$^{ERT2/-}$ BMT animals significantly impaired growth of LLC tumors compared with controls (~50% by day 14; Supplementary Fig. S1B). Impaired growth of these tumors was associated with >2-fold reduction in vessel density (Supplementary Fig. S1C). Further analysis showed that administration of 4-OHT ablated Dicer protein in VE-cadherin$^+$ cells in the bone marrow (Fig. 1A). These results suggested that bone marrow Dicer ablation-mediated suppression of tumor growth and angiogenesis may be because of global miRNA loss.

After having observed a tumor phenotype after global Dicer ablation in the bone marrow, we used a more focused approach to determine the contribution of miRNAs in EPC-mediated tumor angiogenesis. To accomplish this, we exploited our previously established selectivity of the Id1 proximal promoter (Id1pr/p) for EPCs (4). We used the Id1pr/p to express Cre-ERT2 in lineage negative (Lin$^-$) bone marrow–derived cells harvested from Dicer$^{flox/flox}$ mice, so that Dicer ablation in EPCs could be accomplished. The Lin$^-$ Dicer$^{flox/flox}$ bone marrow cells transduced with lentivirus LV-Id1pr/p-GFP-IRES-Cre^{ERT2} (Supplementary Fig. S2A–S2C) were transplanted into irradiated C57BL/6 recipients to generate Dicer$^{flox:flox}$:Id1pr/p-Cre^{ERT2} BMT mice (Supplementary Fig. S3A). After 8 weeks of bone marrow engraftment, flow cytometry analysis of bone marrow from these reconstituted mice showed that as expected approx. 5% of the bone marrow cells express GFP, and that the GFP/CRE^{ERT2} expression was confined to c-kit$^+$ bone marrow cells (Supplementary Fig. S3B). Analysis of LLC tumors in Dicer$^{flox:flox}$:Id1pr/p-Cre^{ERT2} BMT mice showed that the GFP/CRE^{ERT2} expression was restricted to the VE-cadherin$^+$ EPCs in the tumor–stroma (Supplementary Fig. S3C). Treatment of Dicer$^{flox:flox}$:Id1pr/p-Cre^{ERT2} BMT animals with 4-OHT resulted in reduced tumor growth and vessel density, phenocopying conditional Dicer ablation in the whole bone marrow (Fig. 1B). To evaluate this phenotype further, we examined c-kit$^+$ peripheral blood mononuclear cells (PBMC, day 8) and bone marrow mononuclear cells (BMMNC). Notably, a significant reduction in both circulating EPCs (CEP, $P = 0.0022$) and bone marrow EPCs ($P = 0.0286$) was observed in Dicer$^{flox/flox}$:Id1pr/p-Cre^{ERT2} BMT animals treated with 4-OHT (Fig. 1C and D). Importantly, CD11b$^+$ myeloid progenitors remained unchanged, which is consistent with exquisite specificity of Id1pr/p for EPCs (Fig. 1C and D; see also Supplementary Fig. S4A and S4B). As expected, *Dicer* expression was retained in other BMMNCs cells, and not in VE-cadherin$^+$ EPCs of 4-OHT treated Dicer$^{flox/flox}$:Id1pr/p-Cre^{ERT2} BMT animals (Supplementary Fig. S3D). Taken together, these findings suggest that functional Dicer is required for bone marrow–mediated tumor angiogenesis and that EPC-mediated tumor angiogenesis may be dependent on miRNAs generated by Dicer.

miR-10b and miR-196b are upregulated in EPCs in the bone marrow, peripheral blood, and in the tumor bed

To identify candidate miRNAs that contribute to EPC-mediated tumor angiogenesis, we conducted genome-wide small RNA 'deep' sequencing on flow cytometry sorted EPCs from LLC tumors. Reference data from tumor associated myeloid progenitor cells and Lin$^-$ bone marrow–derived cells was also generated (Fig. 2A; Supplementary Tables S1 and S2). miRNAs that were specifically upregulated in EPCs, compared with other bone marrow–derived lineages, and that have been previously implicated in cancer or stem cell biology were selected for further validation by quantitative PCR (qPCR) (Fig. 2B and C; Supplementary Table S3). Among the qPCR validated miRNAs, we selected for further analysis miR-132, which was previously implicated in tumor angiogenesis (34); and miR-10b and miR-196b, which are regulators of the HOX developmental pathway, and have also been implicated in cancer metastasis and angiogenesis (15–17, 35, 36).

Next, *ISH* with LNA probes confirmed the results of qPCR by showing that miR-10b and miR-196b are expressed in EPCs in BMMNCs, PBMCs, and LLC tumor bed (Fig. 2D and E; Supplementary Fig. S5A–S5C). To accurately evaluate EPCs in the tumor bed, we used Id1$^{+/GFP}$ BMT animals in which EPCs are genetically marked with GFP transgene in the bone marrow compartment (4, 19). In these mice, GFP$^+$ EPCs recruited in the LLC tumor showed distinct miR-10b and miR-196b expression (Supplementary Fig. S5D). We also evaluated whether EPCs in other tumor models expressed miR-10b and miR-196b. Consistent with the LLC model, EPCs in orthotopic 4T1 mammary tumors (Supplementary Fig. S5E) and MDA-MB-231 human breast tumors (Supplementary Fig. S5F) showed miR-10b and miR-196b expression by ISH. Notably, levels of miR-10b was found to be reduced in the tumors of 4-OHT–treated Dicer$^{flox/flox}$:Id1pr/p-Cre^{ERT2} BMT animals, whereas its downstream target HOXD10 (36) was found to be upregulated in tumor-associated EPCs (Supplementary Fig. S6A–S6C). Similarly, miR-196b was also reduced in the tumors of 4-OHT treated Dicer$^{flox/flox}$:Id1pr/p-Cre^{ERT2} BMT animals (data not shown). Taken together, these findings indicate that tumor EPCs exhibit a unique miRNA profile compared with other bone marrow–derived

Published OnlineFirst July 25, 2012; DOI:10.1158/0008-5472.CAN-12-0271

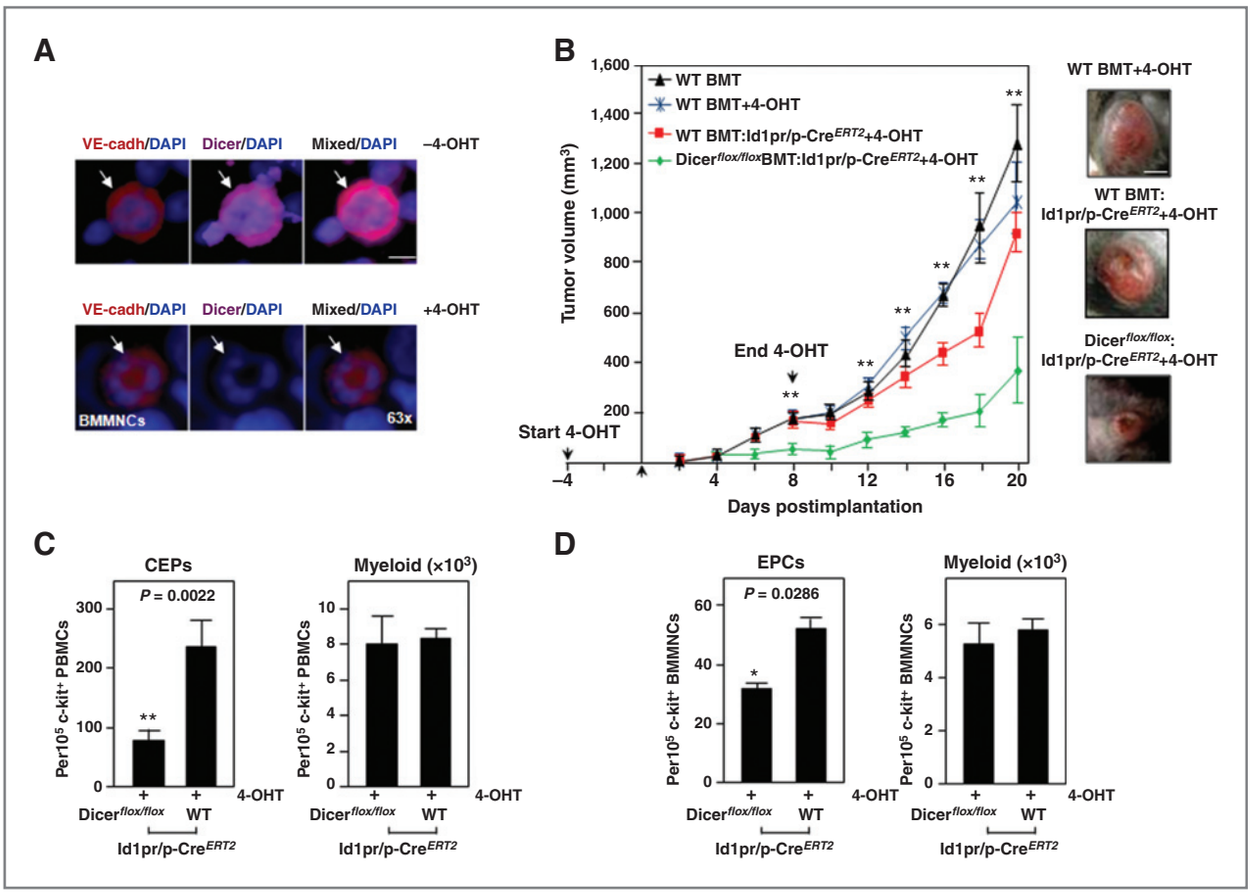

Figure 1. Selective elimination of Dicer in bone marrow EPCs impairs tumor growth. A, high (×63) resolution image of c-kit$^+$ bone marrow cells sorted from tumor challenged Dicer$^{flox/flox}$/Cre$^{ERT2/-}$ BMT animals treated with 4-OHT, showing Dicer is ablated from VE-cadherin$^+$ EPCs (arrows). Scale bar, 10 μm. B, growth of LLC in animals transplanted with Dicer$^{flox/flox}$ bone marrow transduced with Id1pr/p-GFP-IRES-Cre^{ERT2} (Dicer$^{flox/flox}$:Id1pr/p-Cre^{ERT2}) and treated with 4-OHT (mean ± S.E.M., $n = 10$) compared with WT BMT (±4-OHT) and WT:Id1pr/p-Cre^{ERT2} BMT animals treated with 4-OHT. Data analyzed by MANOVA ($\alpha = 0.05$, **, $P < 0.01$). Right, tumor morphology at end point. Scale bar, 20 mm. C, FACS analysis of c-kit$^+$ PBMCs from tumor challenged Dicer$^{flox/flox}$:Id1pr/p-Cre^{ERT2} BMT animals compared with WT:Id1pr/p-Cre^{ERT2} BMT control animals, both treated with +4-OHT, showing significant reduction in the number of mobilized c-kit$^+$ VEGFR2$^+$ CEPs. No significant change was observed in the number of circulating c-kit$^+$ CD11b$^+$ myeloid progenitors. Data analyzed by unpaired t test ($\alpha = 0.05$, *, $P < 0.05$). D, FACS analysis of c-kit$^+$ BMMNCs from tumor challenged Dicer$^{flox/flox}$:Id1pr/p-Cre^{ERT2} BMT mice compared with WT:Id1pr/p-Cre^{ERT2} BMT animals, both treated with 4-OHT, showing number of c-kit$^+$ VEGFR2$^+$ EPCs are significantly decreased in the Dicer$^{flox/flox}$:Id1pr/p-Cre^{ERT2} BMT mice and no difference in c-kit$^+$ CD11b$^+$ myeloid progenitors. For C and D, data are mean number of cells per 1×10^5 ± SEM ($n = 5$ per group); and analyzed by unpaired t test ($\alpha = 0.05$).

lineages, and that the tumor EPC expression of miR-10b and miR-196b may play a functional role in tumor biology *in situ*.

EPC-specific miRNAs are differentially expressed in tumor endothelial cells

To determine if miRNAs, including miR-10b and miR-196b, identified in EPCs were also differentially expressed in tumor endothelial cells, we carried out deep sequencing of small RNAs isolated from the vasculature of tumor and normal tissues (lung and dermis). Comparison of tumor vasculature to normal vasculature showed that several miRNAs were upregulated in the tumor vasculature including miR-10b and miR-196b, and several miRNAs were downregulated in tumor vasculature including miR-451, miR-128, and miR-486 (Fig. 3A; Supplementary Tables S4 and S5A). Furthermore, validation by qPCR showed a remarkable concordance in miRNA expression levels with that of deep sequencing analysis. Moreover, this concordance was preserved in various tumor types examined (Fig. 3B; Supplementary Table S5B). miR-132, previously shown to be associated with tumor endothelial cells (34), was also significantly upregulated in tumor vasculature. To exclude the possibility that contaminating tumor cells may have artificially contributed to the miRNA expression level detected in tumor vasculature, we generated LLC tumors expressing mCherry. From these mCherry$^+$ LLC tumors, tumor cells were excluded and endothelial cells purified using FACS. Importantly, analysis of purified tumor endothelial cells by qPCR and *ISH* showed expression of candidate miRNAs including miR-10b and miR-196b consistent with previous analysis (Supplementary Fig. S7A and B and Table S5C).

ISH analysis of LLC, 4T1, and MDA-MB-231 tumors showed preferential expression of miR-10b (Fig. 3C; Supplementary

Published OnlineFirst July 25, 2012; DOI:10.1158/0008-5472.CAN-12-0271

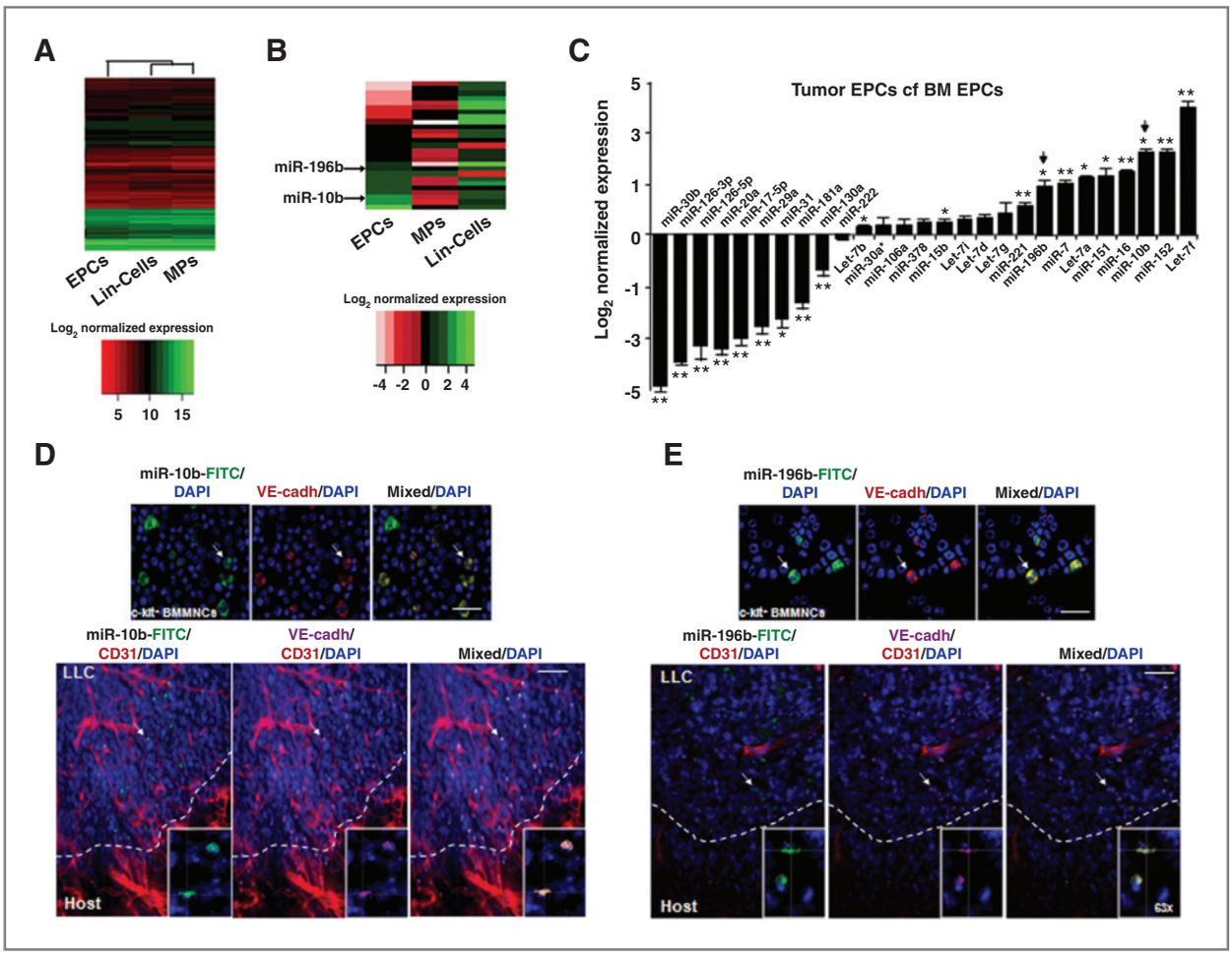

Figure 2. MiR-10b and MiR-196b are upregulated in bone marrow–derived tumor EPCs. A, heat map showing normalized miRNA profile of c-kit$^+$ VE-cadherin$^+$ VEGFR2$^+$ EPCs and c-kit$^+$ VEGFR2$^-$CD11b$^+$ myeloid progenitors (MPs) or c-kit$^+$ VEGFR2$^-$ CD11b$^-$ lineage depleted (Lin$^-$) cells (see also Supplementary Tables S1 and S2). B, heat map showing relative $\log_2$ fold change in miRNA expression levels in bone marrow populations following tumor challenge. C, bar graph showing relative difference in miRNA levels in EPCs in the context of tumor challenge as determined by qPCR. miR-10b and miR-196b are indicated (arrows). Data are mean ± SEM and analyzed by unpaired *t* test ($\alpha = 0.05$, *, $P < 0.05$, **, $P < 0.01$). D, upper, *ISH* image of c-kit$^+$ BMMNCs cells showing miR-10b expression in VE-cadherin$^+$ EPCs (arrow). Scale bar, 20 μm. Lower, *ISH* image of LLC (day 14 postinoculation) showing miR-10b expression in VE-cadherin$^+$ EPCs (arrow) at the tumor host boundary (dotted line). Scale bar, 100 μm. Also shown, CD31$^+$ vasculature and high resolution (×63) miR-10b$^+$ EPC (inset). E, upper, *ISH* image of c-kit$^+$ BMMNCs cells showing miR-196b in VE-cadherin$^+$ EPCs (arrow). Scale bar, 20 μm. Lower, *ISH* image of LLC (day 14) showing miR-196b expression in VE-cadherin$^+$ EPCs (arrow) at the tumor host boundary. Scale bar, 100 μm. Also shown, CD31$^+$ vasculature and high (×63) resolution miR-196b$^+$ EPCs (inset).

Fig. S8A and S8B), miR-196b, and miR-132 (data not shown) in tumor vasculature, compared with vasculature from normal tissues (Supplementary Fig. S8C and S8D). Cytoplasmic expression of miR-10b in tumor endothelium was confirmed by counterstaining with F-actin stain, phalloidin (Supplementary Fig. S9A). Although, in contrast, miR-451 was downregulated in tumor vasculature and was expressed at a relatively high level in normal, nontumor vasculature (Supplementary Fig. S9B).

To obtain insights into whether the candidate miRNAs, identified earlier, were upregulated in the tumor vasculature in response to paracrine activity of the tumor cells, we treated murine endothelial cells with tumor-conditioned medium and observed differential regulation of miR-10b, miR-196b, and miR-132 (Fig. 3D; Supplementary Table S6A). Given that tumor-secreted VEGF has been known as major proangiogenic cytokine that activates endothelial cells, we hypothesized that VEGF may induce miRNA expression in endothelial cells. Indeed, treatment of endothelial cells with VEGF resulted in upregulation of miR-10b (Fig. 3E; Supplementary Table S6B), as well as miR-132 (Supplementary Table S6B). These results show that certain miRNAs such as miR-10b and miR-196 are upregulated in tumor endothelial cells in response to tumor produced growth factors, including VEGF.

miR-10b and miR-196 are expressed in the vasculature of human tumors

To compare our observations in murine tumors to human tumors, we next determined if miR-10b and miR-196b are also involved in human breast cancer. We examined the vasculature of invasive infiltrating ductal carcinoma (IDC) grade III

Published OnlineFirst July 25, 2012; DOI:10.1158/0008-5472.CAN-12-0271

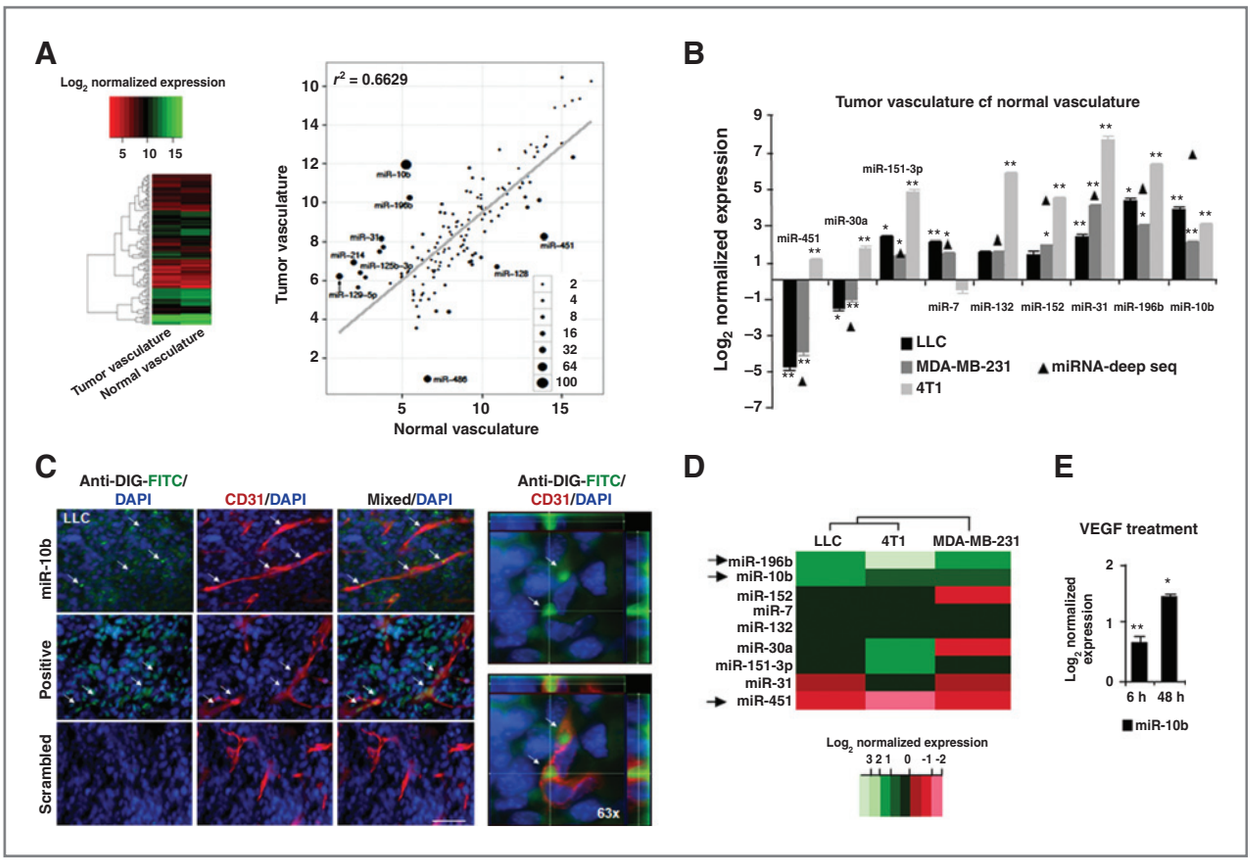

Figure 3. miR-10b and miR-196b are upregulated in tumor vasculature. A, left, heat map showing normalized miRNA profile of tumor vasculature and normal vasculature obtained from deep sequencing. Right, pairwise comparison of miRNA expression showing similarities and differences ($r^2 = 0.6629$, Pearson correlation) in miRNA levels between tumor and normal vasculature results. miRNAs regulated >4-fold are shown. B, qPCR comparison of miRNAs isolated from $CD31^+$ $CD11b^-$ tumor vasculature from LLC (day 14), 4T1 (day 21), and MDA-MB-231 (day 28) tumors compared with $CD31^+$ $CD11b^-$ vasculature from normal wild-type mice. Correlation of qPCR data in the different tumor models with deep sequencing analysis: LLC, $r = 0.9188$; 4T1, $r = 0.5424$; and MDA-MB-231, $r = 0.9128$ by Pearson correlation. Data are mean Log_2(fold) ± SEM and analyzed by unpaired *t* test ($\alpha = 0.05$, *, $P < 0.05$, **, $P < 0.01$). C, left, top, *ISH* showing expression of miR-10b in $CD31^+$ vasculature of LLC (day 14, arrows). Scale bar, 100 μm. Middle, positive control (U6) expression (arrows); bottom, absence of signal by the scrambled control. Right, high (×63) resolution image of miR-10b expressing $CD31^+$ tumor endothelial cell. DIG is digoxigenin. D, heat map showing log_2 normalized changes as determined by qPCR in miRNA levels in murine endothelial cells in response to tumor-conditioned medium from LLC, 4T1, or MDA-MB-231 cells. miR-10b, miR-196b, and miR-451 are indicated with arrows. E, qPCR analysis showing an increase in miR-10b levels in murine endothelial cells after administration of VEGF at 6 and 48 hours. Data are mean Log_2 (fold) ± SEM and analyzed by unpaired *t* test ($\alpha = 0.05$, *, $P < 0.05$, **, $P < 0.01$).

tumors, which showed sentinel lymph node involvement, and localized ductal carcinoma *in situ* (DCIS) that did not present lymph node involvement (20). mir-10b and miR-196b were found to be highly expressed in the vasculature of IDC grade III tumors (Fig. 4A; Supplementary Fig S10A and S10B), with little or no endothelial expression in DCIS tumors (Fig. 4B). Consequently, the number of miR-10b- and miR-196b–expressing tumor vessels was higher in IDC tumors compared with DCIS (Supplementary Fig. S10C and S10D and Table S7A). In agreement with the previous observation, treatment of human endothelial cells with either tumor conditioned media or VEGF resulted in the upregulation of miR-10b and miR-196b (Fig. 4C and D; Supplementary Fig. S10E and Tables S7B and S7C). These results show that miR-10b and miR-196 are preferentially expressed in the vasculature of more invasive human breast tumors, and that they are upregulated by tumor produced growth factors in human endothelial cells.

Suppression of miR-10b and miR-196b decreases endothelial cell migration and tubule formation *in vitro*

It has previously been shown that the downstream target of miR-10b, HOXD10 inhibits endothelial cell migration and angiogenesis (36, 37). In this study, we found that HoxD10 is upregulated in EPCs impaired for miRNA biogenesis (Supplementary Fig. S6); therefore, to determine whether miRNA regulation of Hox signaling plays a role in angiogenesis, we used anti-miRs to inhibit either miR-10b or miR-196b and examined the effect on HOXD10 levels and endothelial cell function in human and murine endothelial cells *in vitro* (37). We used Cy3-conjugated anti-miRs to confirm efficient transfection of murine and human endothelial cells (Supplementary Fig. S11A and S11B). Notably, suppression of both miR10b and miR-196b lead to significantly reduced endothelial cell tube number and tube length compared with controls (~20–30% reduction; Fig. 5A and B; Supplementary Fig. S11C and Table

Published OnlineFirst July 25, 2012; DOI:10.1158/0008-5472.CAN-12-0271

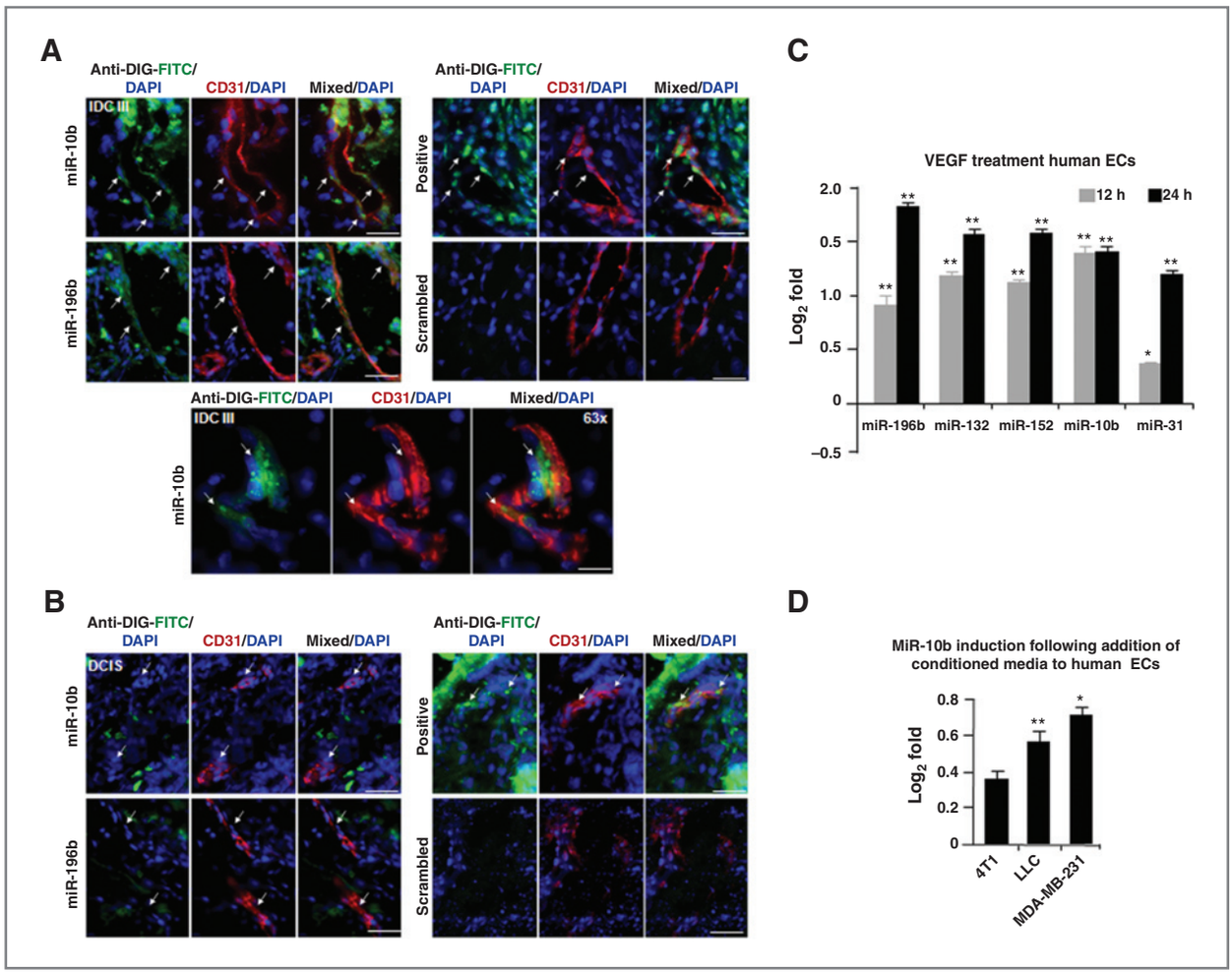

Figure 4. miR-10b is expressed in the vasculature of high-grade human breast tumors. A, *ISH* showing miR-10b and miR-196b expression in $CD31^+$ vasculature (arrows) within IDC grade III human tumor biopsies. Also shown, positive and scrambled probe controls. Scale bar, 100 μm. Lower, high (×63) resolution image of miR-10b expression in $CD31^+$ tumor endothelial cell in IDCIII breast tumor biopsy. B, *ISH* showing limited expression of miR-10b and miR-196b in $CD31^+$ vasculature (arrows) within more contained DCIS human tumor biopsy. Scale bar, 100 μm. C, qPCR analysis showing VEGF induction of miRNAs at 12 and 24 hours posttreatment in human endothelial cells. D, qPCR analysis showed induction of miR-10b (∼80%) in human endothelial cells by tumor-conditioned media collected from 4T1, LLC, and MDA-MB-231 cell cultures. For C and D, data are mean Log_2 (fold) ± SEM and analyzed by unpaired *t* test ($\alpha = 0.05$, *, $P < 0.05$, **, $P < 0.01$).

S8–S8D),; as well as impaired migration of human and murine endothelial cells in wound healing assays (Supplementary Fig. S11D and Table S8E–S8H). Furthermore, suppression of miR-10b led to an increase in HOXD10, which was further confirmed by assessing its downstream target miR-7 that was upregulated in human and mouse endothelial cells (Fig. 5C; Supplementary Fig. S11E and Supplementary Methods; ref. 38). Notably, suppression of miR-196b also led to increased HOXD10, a finding that has not been previously reported, whereas levels of HOXA9 (39) remained unchanged (Fig. 5C).

Administration of anti-miR-10b and anti-miR-196b results in EPC-mediated impaired tumor growth *in vivo*

After having established that suppression of miR-10b and miR-196b leads to endothelial cell dysfunction, we next determined the effects of miR-10b and miR-196b suppression on angiogenesis-mediated tumor growth *in vivo*. We administered anti-miRs using RGD incorporated "stealth liposomes" (34,40) intravenously to target the tumor vasculature in mice bearing 4T1 tumors. The RGD-peptide, which recognizes intergin $\alpha_v\beta_3$, expressed by tumor vasculature, was conjugated to cholesterol, separated by a polyethylene glycol (2xPEG) linker, and incorporated into liposomes with FITC-labeled anti-miRs, using the hydration of freeze dried matrix method (ref. 40; Supplementary Methods and Fig. S12A). Notably, anti-miR-10b treated mice showed significantly reduced tumor volume and weight (Fig. 5D). Two days after last treatment, significant FITC signal was detected in mononuclear cells from the bone marrow (∼5% of BMMNCs), peripheral blood (∼0.08% of PBMCs; Supplementary Fig. S12B), and tumor vasculature (Supplementary Fig. S12C). This was associated with a significant reduction in the number of CEPs, but no change in myeloid cells in either

Published OnlineFirst July 25, 2012; DOI:10.1158/0008-5472.CAN-12-0271

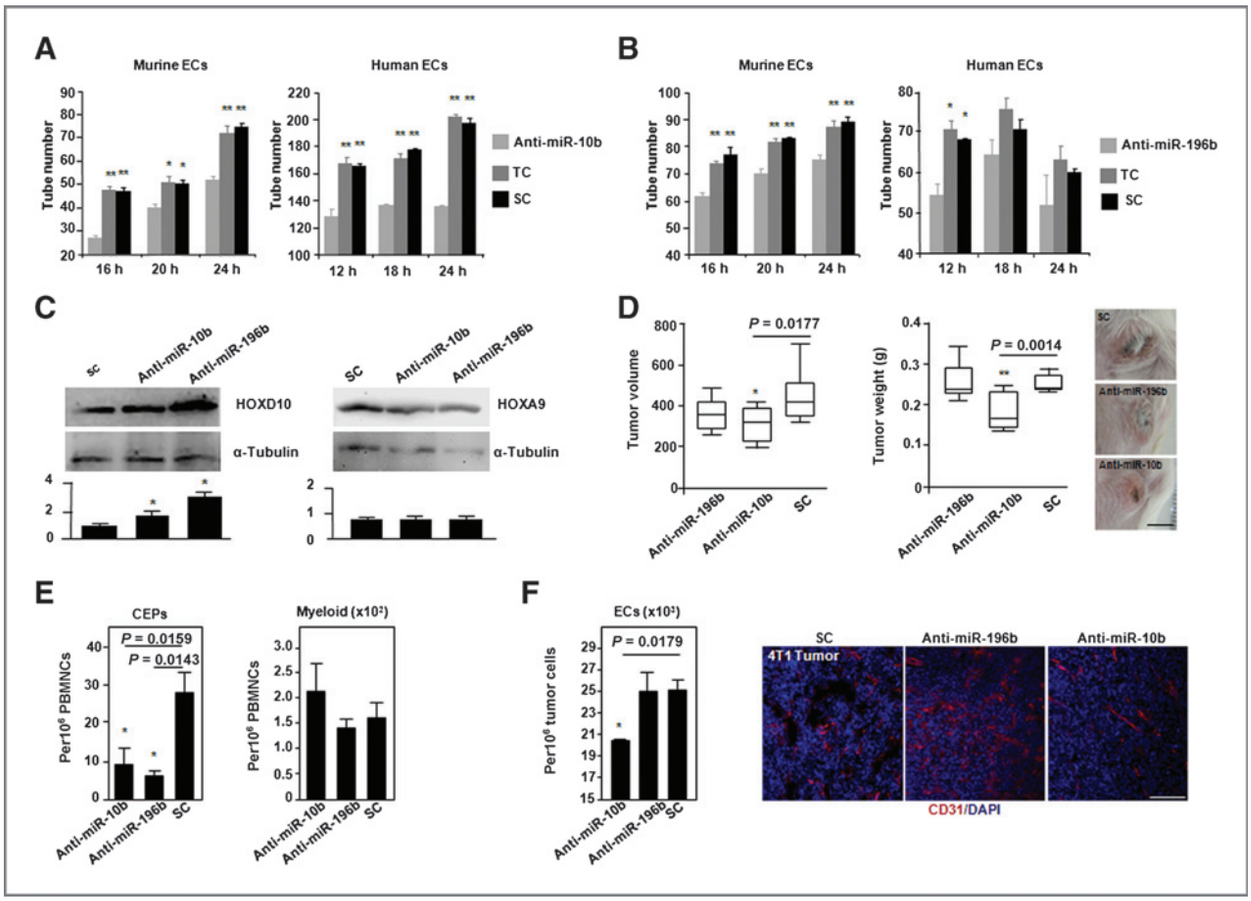

Figure 5. miR-10b and miR-196b are required for endothelial cell function. A, tube formation assay after suppression of miR-10b, showing reduced tube number in anti-miR–treated murine (left) and human (right) endothelial cells compared with transfection reagent treated (TC) and scrambled (SC) controls. B, tube formation assay after suppression of miR-196b showing impaired tube number in anti-miR–treated murine (left) and human (right) endothelial cells compared with TC and SC. For A and B, data are mean tube number ± SEM and analyzed by unpaired *t* test ($\alpha = 0.05$, *, $P < 0.05$, **, $P < 0.01$). C, Western blot analysis of human endothelial cells showing an increase in levels of HOXD10 protein (40 kDa) after suppression of miR-10b and miR-196b. Upper right, levels of HOXA9 (35 kDa) remained unchanged. Below, normalized relative quantitative differences in HOX levels. Data are relative pixel density, compared with background ± SEM, compared with SC, and analyzed by unpaired *t* test ($\alpha = 0.05$, *, $P < 0.05$). D, RGD directed delivery of liposomes carrying anti-miR10b and anti-miR196b via tail vein injection on orthotopic 4T1 tumor growth. Left, significantly impaired tumor volume; right, significantly impaired tumor weight in anti-miR-10b treated animals. Data are box plots with medium tumor volume indicated and analyzed by Mann–Whitney *U* test ($\alpha = 0.05$, *, $P < 0.05$, **, $P < 0.01$). Representative images of tumors from each category are shown at the right. Scale bar, 10 mm. E, FACS analysis of peripheral blood showing a significant decrease in the number of c-kit$^+$VEGFR2$^+$ CEPs compared with c-kit$^+$CD11b$^+$ myeloid progenitors. F, left, FACS analysis of tumors showing a significant decrease in the number of CD31$^+$CD11b$^-$ endothelial cells. Right, fluorescent microscopy images showing vessel density in 4T1 tumors in mice treated with anti-miR–treated and scrambled. Scale bar, 100 μm.

anti-miR-10b or anti-miR-196b treated mice was found (Fig. 5E and Supplementary Fig. S12D). Notably, tumors from anti-miR-10b treated mice showed a significantly reduced number of tumor endothelial cells; as well as phenotypic changes in tumor vasculature (Fig. 5F). Taken as a whole these data suggests that targeting miR-10b leads to significant EPC defects as well as a reduction in tumor growth.

Discussion

Although the contribution of miRNAs to tumor angiogenesis has been reported (7, 13, 34), the challenge of delivering transgenes to specific cell types in the bone marrow–compartment of tumor–stroma has precluded study of the biological function of EPC miRNAs and has impaired attempts to obtain a deeper understanding of their clinical significance. Furthermore, although EPC-associated miRNAs have been reported through *in vitro* studies (e.g., miR-34a; ref. 41), there has, as yet, been no direct link made between their expression by EPCs, and their significance to tumor vascular biology *in vivo*.

It is known that Dicer-regulated miRNA biogenesis is a key factor in normal cell function, embryological development, and stem cell biology (17). In this study, we have used Dicer^{floxed} mice and exploited the selectivity of the Id1 proximal promoter-LV reporter (4) to mark EPCs to show for the first time that Dicer is required for EPC-mediated tumor angiogenesis (Fig. 1). This result concurs with a related finding that Dicer is required for vascular integrity during embryogenesis (14).

Published OnlineFirst July 25, 2012; DOI:10.1158/0008-5472.CAN-12-0271

To identify which miRNAs may be required for EPC-mediated tumor angiogenesis, we conducted small RNA deep sequencing analysis of EPCs, bone marrow–derived myeloid cells, and undifferentiated c-kit$^+$ cells (Fig. 2A and B). These experiments revealed for the first time, an EPC-intrinsic miRNA signature that phenotypically distinguishes tumor EPCs from myeloid cells and Lin$^-$ bone marrow–derived cells. Of more than 100 miRNAs that were identified as differentially regulated in tumor-EPCs, several have been linked previously to endothelial cell function, including miR-221, that is believed to mediate release of EPCs from the bone marrow by regulating c-kit (7, 13, 14). Other miRNAs, such as miR-152, have not yet been linked to vascular biology but have been shown to have functions such as regulation of DNA methylation (42). miR-10b and miR-196b were also upregulated in EPCs from the blood, bone marrow, and the tumor–stroma in syngeneic and human xenograft tumor mouse models (Fig. 2D and E). Both of these miRNAs have previously been implicated in development and cancer biology (15–17, 36). Notably, miR-126-3p and 5p, which inhibit proliferation (43), were significantly downregulated in EPCs that are known to expand and mobilize into the peripheral blood in response to tumor cytokines (2).

To identify how closely the EPC miRNA signature resembles that of tumor vasculature, a second round of deep sequencing and qPCR analysis was conducted on mature endothelial cells, isolated from tumor vasculature (Fig. 3). In agreement with our findings in EPCs, both miR-10b and miR-196b were significantly upregulated (8- to 100-fold) in tumor vasculature, whereas miR-451, an important tumor suppressor in lung cancer (44, 45), was significantly downregulated in tumor vasculature. Notably, both miR-10b and miR-196b were found to be positively regulated by tumor-conditioned medium; and miR-10b, like miR-132 was regulated by VEGF, in murine endothelial cells *in vitro*. Human endothelial cells in culture also showed increased levels of miR-10b and miR-196b, in response to tumor-conditioned medium and miR-10b levels were increased in response to VEGF (Fig. 4). These results are supported by recent observations, which show that: (i) HoxD10 (coexpressed with miR-10b) is coregulated with VEGF in cancer (46); and (ii) that HoxA9 (coexpressed with miR-196b) is a downstream target of VEGFR2 signaling (47). This data strongly indicate that miR-10b and miR-196b may also have a significant role in both EPC function and tumor angiogenesis. In fact, suppression of miR-10b and miR-196b led to significant defects in tube number, length, and mobilization in human and murine endothelial cells (Fig. 5) in agreement with a recent observation showing that miR-10b regulates HOXD10 in microvessels (35). HOXD10 has been showed to suppress angiogenesis (37). Here we show that the levels of HOXD10, and its target miR-7, were increased following suppression of miR-10b or miR-196b (Fig. 5C and Supplementary Fig. S11E). The regulation of HOXD10 by miR-196b has not previously reported. However, as there are no predicted binding sites for miR-196b in HOXD10 (not shown), regulation of HOXD10 by miR-196b is likely to be indirect. Taken as a whole these findings show that miR-10b and miR-196b are involved in EPC function and tumor angiogenesis through modulation of the Hox pathway.

Recently, the role of metastasis-linked miRNAs has been controversial. Although there is a strong link between miR-10b, the epithelial-to-mesenchymal transition (EMT), and tumorigenesis (36, 48), authors such as Gee and colleagues (49) did not find a correlation between miR-10b levels and node involvement, and no direct link with patient outcome. Furthermore, in 2010, Ma and colleagues (50) showed reduced metastasis in the mouse 4T1 breast tumor model following suppression of miR-10b by systemic delivery of an antagomir/anti-miR. They concluded that rare malignant tumor cells that had undergone an EMT were the main target of "anti-miR-10b," and that these are difficult to detect in patient samples. In this paper, we have showed for the first time that vasculature from invasive IDC grade III tumors showed consistently higher levels of miR-10b and miR-196b expression compared with endothelial cells that were detected in less malignant DCIS biopsies (Fig. 4; ref. 20), suggesting that vascular expression of miR-10b and miR-196b may be indicative of metastatic progression and patient outcome in breast cancer. Furthermore, as EPCs are required for the growth of primary tumors and metastases (2–6), reduced metastasis following inhibition of miR-10b, observed by Ma and colleagues (50) could also be a result of impaired EPC-mediated angiogenesis. Indeed, we have now showed that RGD-directed liposomal delivery of anti-miR-10b results in breast tumor growth impairment, as well as reduced levels of CEPs (Fig. 5).

In conclusion, by localizing the expression of miRNAs to EPCs and vasculature, we have showed that miR-10b and miR-196b are key players in EPC biology and tumor angiogenesis. Anticancer therapies targeting either of these miRNAs may, not only prevent malignant progression mediated by the EMT, but may also significantly delay tumor growth by inhibiting the angiogenic switch in primary tumors and metastases.

Disclosure of Potential Conflicts of Interest

No potential conflicts of interest were disclosed.

Authors' Contributions

Conception and design: P.N. Plummer, C.A. Johns, A. Swarbrick, V. Mittal, A.S. Mellick

Development of methodology: P.N. Plummer, D. Gao, C.A. Johns, N.A. McMillan, A.S. Mellick

Acquisition of data (provided animals, acquired and managed patients, provided facilities, etc.): P.N. Plummer, R. Freeman, J. Vider, M. Sax, C.A. Johns, N.A. McMillan, A. Swarbrick, V. Mittal, A.S. Mellick

Analysis and interpretation of data (e.g., statistical analysis, biostatistics, computational analysis): P.N. Plummer, R. Freeman, R. Taft, J. Vider, V. Mittal, A.S. Mellick

Writing, review, and/or revision of the manuscript: P.N. Plummer, R. Freeman, R. Taft, J. Vider, M. Sax, B. A. Umer, C.A. Johns, J.S. Mattick, A. Swarbrick, V. Mittal, A.S. Mellick

Administrative, technical, or material support (i.e., reporting or organizing data, constructing databases): P.N. Plummer, R. Freeman, M. Sax, C.A. Johns, S.D. Wilton

Study supervision: V. Mittal, A. S. Mellick

Acknowledgments

The authors thank Pamela Moody and Lisa Bianco (Cold Spring Harbor Laboratory), Grace Chojnowski (Queensland Institute of Medical Research), Robert King (GeneWorks), Dianne Muller (Zeiss), Bernadette Bellette, Daniel Clarke, and Cameron Flegg (Griffith University), as well as Jana McCaskill and Sherry Wu (University of Queensland).

Published OnlineFirst July 25, 2012; DOI:10.1158/0008-5472.CAN-12-0271

Grant Support

This work was supported by grants held by Albert Mellick and Vivek Mittal from the Australian Research Council, Queensland Cancer Council, Surfers Sunrise Rotary, the National Health and Medical Research Council, and the National Institutes of Health. Alexander Swarbrick is the recipient of an Early Career Fellowship from the National Breast Cancer Foundation, Australia. Funders had no role in study design, data collection, analysis, decision to publish, or manuscript preparation.

The costs of publication of this article were defrayed in part by the payment of page charges. This article must therefore be hereby marked *advertisement* in accordance with 18 U.S.C. Section 1734 solely to indicate this fact.

Received January 25, 2012; revised July 11, 2012; accepted July 11, 2012; published OnlineFirst July 25, 2012.

References

1. Folkman J. Role of angiogenesis in tumor growth and metastasis. Semin Oncol 2002;29:15–8.
2. Nolan DJ, Ciarrocchi A, Mellick AS, Jaggi JS, Bambino K, Gupta S, et al. Bone marrow-derived endothelial progenitor cells are a major determinant of nascent tumor neovascularization. Genes Dev 2007;21:1546–58.
3. Gao D, Nolan DJ, Mellick AS, Bambino K, McDonnell K, Mittal V. EPCs control the angiogenic switch in mouse lung metastasis. Science 2008;319:195–8.
4. Mellick AS, Plummer PN, Nolan DJ, Gao D, Bambino K, Hahn M, et al. Using the transcription factor inhibitor of DNA binding 1 to selectively target endothelial progenitor cells offers novel strategies to inhibit tumor angiogenesis and growth. Cancer Res 2010;70:7273–82.
5. Kopp HG, Ramos CA, Rafii S. Contribution of endothelial progenitors and proangiogenic hematopoietic cells to vascularization of tumor and ischemic tissue. Curr Opin Hematol 2006;13:175–81.
6. Asahara T, Takahashi T, Masuda H, Kalka C, Chen D, Iwaguro H, et al. VEGF contributes to postnatal neovascularization by mobilizing bone marrow derived endothelial progenitor cells. EMBO J 1999;18:3964–72.
7. Urbich C, Dimmeler S. Endothelial progenitor cells: characterization and role in vascular biology. Circ Res 2004;95:343–53.
8. Krol J, Loedige I, Filipowicz W. The widespread regulation of microRNA biogenesis, function and decay. Nat Rev Genet 2010;9:597–610.
9. Taft RJ, Glazov EA, Cloonan N, Simons C, Stephen S, Faulkner GJ, et al. Tiny RNAs associated with transcription start sites in animals. Nat Genet 2009;41:572–8.
10. Suarez Y, Sessa WC. MicroRNAs as novel regulators of angiogenesis. Circ Res 2009;104:442–54.
11. Suárez Y, Fernández-Hernando C, Pober JS, Sessa WC. Dicer dependent microRNAs regulate gene expression and functions in human endothelial cells. Circ Res 2007;100:1164–73.
12. Kuehbacher A, Urbich C, Zeiher A, Dimmeler S. Role of Dicer and DROSHA for endothelial microRNA expression and angiogenesis. Circ Res 2007;101:59–68.
13. Urbich C, Kuehbacher A, Dimmeler S. Role of microRNAs in vascular diseases, inflammation, and angiogenesis. Cardiovasc Res 2008;79:581–8.
14. Yang WJ, Yang DD, Na S, Sandusky GE, Zhang Q, Zhao G. Dicer is required for embryonic angiogenesis during mouse development. J Biol Chem 2005;280:9330–5.
15. Tehler D, Høyland-Kroghsbo NM, Lund AH. The miR-10 microRNA precursor family. RNA Biol 2011;8:728–34.
16. Lund AH. miR-10 in development and cancer. Cell Death Differ 2010;17:209–14.
17. O'Connell RM, Rao DS, Chaudhuri AA, Baltimore D. Physiological and pathological roles for microRNAs in the immune system. Nat Rev Immunol 2010;10:111–22.
18. Murchison EP, Partridge JF, Tam OH, Cheloufi S, Hannon GJ. Characterization of dicer-deficient murine embryonic stem cells. Proc Natl Acad Sci USA 2005;102:12135–40.
19. Perry SS, Zhao Y, Nie L, Cochrane SW, Huang Z, Sun XH. Id1, but not Id3, directs long-term repopulating hematopoietic stem cell maintenance. Blood 2007;110:2351–60.
20. Vargo-Gogola T, Rosen JM. Modelling breast cancer: one size does not fit all. Nat Rev Cancer 2007;7:659–72.
21. Campbell RE, Tour O, Palmer AE, Steinbach PA, Baird GS, Zacharias DA, et al. A monomeric red fluorescent protein. Proc Natl Acad Sci USA 2002;99:7877–82.
22. Wagner K-U, McAllister K, Ward T, Davis B, Wiseman R, Hennighausen L. Spatial and temporal expression of the Cre gene under the control of the MMTV-LTR in different lines of transgenic mice. Transgenic Res 2001;10:545–53.
23. Tudor KS, Deem TL, Cook-Mills JM. Novel alpha 4-integrin ligands on an endothelial cell line. Biochem Cell Biol 2000;78:99–113.
24. De Palma M, Venneri MA, Galli R, Sergi Sergi L, Politi LS, Sampaolesi M, et al. Tie2 identifies a hematopoietic lineage of proangiogenic monocytes required for tumor vessel formation and a mesenchymal population of pericyte progenitors. Cancer Cell 2005;8:211–26.
25. Salmon P, Kindler V, Ducrey O, Chapuis B, Zubler RH, Trono D, et al. High-level transgene expression in human hematopoietic progenitors and differentiated blood lineages after transduction with improved lentiviral vectors. Blood 2000;96:3392–8.
26. Kloosterman WP, Wienholds E, de Bruijn E, Kauppinen S, Plasterk RH. *In situ* detection of miRNAs in animal embryos using LNA-modified oligonucleotide probes. Nat Methods 2006;3:27–9.
27. Preis M, Gardner TB, Gordon SR, Pipas JM, Mackenzie TA, Klein EE, et al. MicroRNA-10b expression correlates with response to neoadjuvant therapy and survival in pancreatic ductal adenocarcinoma. Clin Cancer Res 2011;17:5812–21.
28. Perfetto SP, Chattopadhyay PK, Roederer M. Seventeen-colour flow cytometry: unraveling the immune system. Nat Rev Immunol 2004;4:648–55.
29. Fahlgren N, Sullivan CM, Kasschau KD, Chapman EJ, Cumbie JS, Montgomery TA, et al. Computational and analytical framework for small RNA profiling by high-throughput sequencing. RNA 2009;15:992–1002.
30. Goecks J, Nekrutenko A, Taylor J The Galaxy Team. Galaxy: a comprehensive approach for supporting accessible, reproducible, and transparent computational research in the life sciences. Genome Biol 2010;11:R86.
31. Langmead B, Trapnell C, Pop M, Salzberg SL. Ultrafast and memory-efficient alignment of short DNA sequences to the human genome. Genome Biol 2009;10:R25.
32. Kozomara A, Griffiths-Jones S. miRBase: integrating microRNA annotation and deep-sequencing data. Nucleic Acids Res 2011;39:D152–7.
33. Rose'Meyer RB, Mellick AS, Garnham BG, Harrison GJ, Massa HM, Griffiths LR. The measurement of adenosine and estrogen receptor expression in rat brains following ovariectomy using quantitative PCR analysis. Brain Res Brain Res Protoc 2003;11:9–18.
34. Anand S, Majeti BK, Acevedo LM, Murphy EA, Mukthavaram R, Scheppke L, et al. MicroRNA-132–mediated loss of p120RasGAP activates the endothelium to facilitate pathological angiogenesis. Nat Med 2010;16:909–14.
35. Shen X, Fang J, Lv X, Pei Z, Wang Y, Jiang S, et al. Heparin impairs angiogenesis through inhibition of microRNA-10b. J Biol Chem 2011;30:26616–27.
36. Ma Li, Teruya-Feldstein J, Weinberg RA. Tumour invasion and metastasis initiated by microRNA-10b in breast cancer. Nature 2007;449:682–8.
37. Myers C, Charboneau A, Cheung I, Hanks D, Boudreau N. Sustained expression of homeobox D10 inhibits angiogenesis. Am J Pathol 2002;161:2099–109.
38. Reddy SD, Ohshiro K, Rayala SK, Kumar R. MicroRNA-7, a homeobox D10 target, inhibits p21-activated kinase 1 and regulates its functions. Cancer Res 2008;68:8195–200.
39. Bruhl T, Urbich C, Aicher D, Acker-Palmer A, Zeiher AM, Dimmeler S. Homeobox A9 transcriptionally regulates the EphB4 receptor to

Published OnlineFirst July 25, 2012; DOI:10.1158/0008-5472.CAN-12-0271

modulate endothelial cell migration and tube formation. Circ Res 2004;94:743–51.
40. Wu SY, Singhania A, Burgess M, Putral LN, Kirkpatrick C, Davies NM, et al. Systemic delivery of E6/7 siRNA using novel lipidic particles and its application with cisplatin in cervical cancer mouse models. Gene Ther 2011;18:14–22.
41. Zhao T, Li J, Chen AF. MicroRNA-34a induces endothelial progenitor cell senescence and impedes its angiogenesis via suppressing silent information regulator 1. Am J Physiol Endocrinol Metab 2010;299: E110–6.
42. Tsuruta T, Kozaki K, Uesugi A, Furuta M, Hirasawa A, Imoto I, et al. miR-152 is a tumor suppressor microRNA that is silenced by DNA hypermethylation in endometrial cancer. Cancer Res 2011;71:6450–62.
43. Meister J, Schmidt MH. miR-126 and miR-126*: new players in cancer. Sci World J 2010;10:2090–100.
44. Wang R, Wang ZX, Yang JS, Pan X, De W, Chen LB. MicroRNA-451 functions as a tumor suppressor in human non-small cell lung cancer by targeting ras-related protein 14 (RAB14). Oncogene 2011;30:2644–58.
45. Rasmussen KD, Simmini S, Abreu-Goodger C, Bartonicek N, Di Giacomo M, Bilbao-Cortes D, et al. The miR-144/451 locus is required for erythroid homeostasis. J Exp Med 2010;207:1351–8.
46. Chen A, Cuevas I, Kenny PA, Miyake H, Mace K, Ghajar C, et al. Endothelial cell migration and vascular endothelial growth factor expression are the result of loss of breast tissue polarity. Cancer Res 2009;69:6721–9.
47. Arao T, Matsumoto K, Furuta K, Kudo K, Kaneda H, Nagai T, et al. Acquired drug resistance to vascular endothelial growth factor receptor 2 tyrosine kinase inhibitor in human vascular endothelial cells. Anticancer Res 2011;31:2787–96.
48. Iorio MV, Ferracin M, Liu CG, Veronese A, Spizzo R, Sabbioni S, et al. MicroRNA gene expression deregulation in human breast cancer. Cancer Res 2005;65:7065–70.
49. Gee HE, Camps C, Buffa FM, Colella S, Sheldon H, Gleadle JM, et al. MicroRNA-10b and breast cancer metastasis. Nature 2008;455:E8–9.
50. Ma L, Reinhardt F, Pan E, Soutschek J, Bhat B, Marcusson EG, et al. Therapeutic silencing of miR-10b inhibits metastasis in a mouse mammary tumor model. Nat Biotechnology 2010;28:341–7.

Supplementary Methods

Transgenic mice. Mice homozygous for the *floxed* allele spanning exon 22 and exon 23 (encoding the *RNase*III domain) of DICER (Dicer$^{flox/flox}$) were provided by E. Murchison (Hannon Lab, CSHL, NY) (18). Dicer$^{flox/flox}$ animals were crossed with mice that carry a conditional *Causes recombination* (CRE) recombinase (Cre-ERT2) allele targeted to the ubiquitously expressed ROSA26 locus (obtained from the Jackson Laboratory, Bar Harbor, Maine). Dicer$^{flox/flox}$ genotyping primers have been previously published (18). A multiplex primer strategy using a Cre-recombinase specific primer set (324bp: *forward*: 5'-CTAGGCCACAGAATTGAAAGATCT-3' & *reverse* 5'-GTAGGTGGAAATTCTAGCATCATCC-3'); as well as internal control (100bp: *forward*: 5'-GCGGTCTGGCAGTAAAAACTATC-3' & *reverse*: 5'-GTGAAACAGCATTGCTGTCACTT-3'), was developed to identify homozygous Dicer$^{flox/flox}$ and heterozygous Cre-ERT2 (Dicer$^{flox/flox}$/Cre$^{ERT2/-}$) progeny. Dicer$^{flox/flox}$/Cre$^{ERT2/-}$ mice were then used as the donors for bone marrow transplantation (BMT). Transgenic mice, which have a single copy of the Id1 allele replaced with green fluorescent protein (GFP), Id1$^{+/GFP}$ (B6.129X1-*Id1*^{tm1Xhsu}/J), previously used to track EPCs in the tumor-stroma (4), were obtained from the Jackson Laboratory (19).

Sample collection of murine tissues for immunohistochemistry (IHC). Mice were sacrificed and subjected to whole animal perfusion with 4% paraformaldehyde (PFA). Selected tissues were cryopreserved in optimal cutting temperature (O.C.T.) medium (Tissue-Tek, Elkhart, IN), and prepared as 10-30μm thick sections. Peripheral blood (PB) was collected from the tail vein in anti-coagulant buffer (PBS, 5mM EDTA), and BM was flushed from the femur and tibia into PBS. PB and BM mononuclear cells (BMMNCs) were isolated by gradient centrifugation using Histopaque 1077 (Sigma Aldrich), and cytospun (Cytocentrifuge Universal 320 Hettich, Leipzig, Germany) onto positively charged Superfrost

Plus Slides (Menzel-Glaser, Braunschweig, Germany). Adherent cell lines were grown on eight chamber culture slides (BD Falcon Franklin Lakes, NJ).

Western Blot Analysis. Endothelial cells were transfected (as described below) then lysed [Lysis buffer: 150mM NaCl, 20mM Tris–HCl (pH 7.4), 1mM EDTA, 1% Triton X-100, 1mg/ml Leupeptin, 1mg/ml Aprotinin, 100 mM PMSF]. After removal of cell debris by centrifugation, protein concentration in cell lysates was determined (Nanodrop1000™, Thermo Scientific). Lysate was then added to loading buffer [0.5M Tris-HCl pH6.8, SDS (2%), 2-Mercaptoethanol (5%), Glycerol (10%), Bromophenol blue (1%)], heated (99°C, 5min), and the proteins separated by 12.5% SDS–PAGE gel. The Cruz Molecular Weight Standard™ (Santa Cruz Biotechnology, Santa Cruz, CA) was run as a size standard. The protein lysates were electrotransferred to PVDF membranes, in Transfer Buffer [25mM Tris, 190mM Glycine, SDS (0.1%), Methanol (20%), pH8.5]. To detect differences in HOXD10 and HOXA9 levels, polyclonal goat anti-HOXD10 (Cat$^{\#}$33005), or anti-HOXA9 (Cat$^{\#}$17156) antibodies, which are cross reactive for mouse and human, were obtained from Santa Cruz Biotechnology. After immunoblotting (1:100, 2h) the membranes were incubated with Horse Radish Peroxidase (HRP)-conjugated anti-goat IgG (1:5000, 2h) (Santa Cruz Biotechnology). Blots were developed with WestPico Supersignal (Pierce Biosciences, Rockford, IL) and chemiluminescence recorded using the ChemiDoc XRS system (Bio-Rad). The membrane was then stripped [SDS (40%), 2-Mercaptoethanol (2%) in Tris-HCl pH6.8] and incubated with mouse monoclonal anti-α-Tubulin (1:10000, 2h) antibody and anti-mouse HRP conjugated IgG (1:5000, 2h), as a sample reference. Normalized relative quantitative difference in HOX levels was determined via analysis of density intensity using Quantity One (Version 4.5, Bio-Rad).

Tubule formation and motility assays. Cells were transfected with anti-miRs using a modified protocol of previously published methods (35). Cells were transfected with

0.04pmol/μl Cy3-labeled antisense RNA oligonucleotide probe (Ambion anti-miRs™, Austin, TX), using siPORT NeoFX Transfection Agent (Ambion). Negative (scrambled) probe, or transfection reagent were used as the controls. To assess the effects of miRNA suppression on tube formation, transfected cells were grown on BD Matrigel™. Tube formation was visualized; tube number and lengths from randomly selected fields were analyzed, using Image J Software (v1.44, NIH, Maryland). For the motility assay, a scratch (wound) was made across a cell monolayer. The cleared area was visualized, recorded and the closing wound area measured using Image J. The cell migration distance, relative to migration rate was determined using the equation $(distance_{t=0h} – distance_{t=24h})/distance_{t=0h} \times 100\%$ (35).

RGD-peptide directed delivery of anti-miRs *in vivo*. To create antimiR-containing, vascular targeting liposomes, cycloRGD peptide (Arg-Gly-Asp-D-Phe-Lys, Peptides International, Louisville, KY) containing two polyethylene glycol (PEG) linkers and conjugated to cholesteryl, was combined with 1,2-dioleoyl-3-trimethylammonium-propane (DOTAP), cholesterol, 1,2-Dioleoyl-sn-Glycero-3-Phosphoethanolamine (DOPE), C8 mPEG 750 Ceramide, (Avanti Polar Lipids, Alabaster, Alabama), in a ratio of 2.5:50:35:5:7.5, using a method adapted from Wu *et al*. (40). For FITC-labeled anti-miR production, 2'-O-methyl modified bases on a phosphorothioate backbone (2'OMeAOs) were prepared on the Expedite 8909 nucleic acid synthesizer (UWA, Australia), targeting: miR-10b-5'-CACAAAUUCGGUUCUACAGGGUA-FITC-3'; miR-196b 5'-CCCAACAACAGGAAACUACCUA-FITC-3'; and control 5'-GCAAGAGCGUAAAACACUUC-FITC-3'. Prior to administration, liposome size and distribution was assessed using a Zetasizer Nano (Malvern Instruments, Worcestershire, UK.). For each experiment 50μg/mouse of FITC labeled anti-miR in RGD-liposomes was injected via tail vein every three days, starting two days after tumour 4T1 cells were inoculated.

Tumors were harvested 2 days after the last treatment, at which time tumour weight, vessel density and EPC contribution was assessed as previously described (4).

Data and statistical analysis. Statistical analysis was performed using GraphPad Prism™ (version 3.0). One-way MANOVA (α=0.05) was used to compare differences in tumor growth curves. For comparison of the different cell populations Unpaired *t* test analysis was used (α=0.05). Quantitative differences in expression by Q-PCR are represented as Log_2(fold) values (or $\Delta\Delta$CT), and significance was determined through comparison of the difference in the two of ΔCT values (one for each matched test and control groups), by Unpaired *t* test (α=0.05) (33). Tube formation and wound healing data were also assessed by Unpaired *t* test analysis, while scoring of tumor vascular miRNA expression in human tumor biopsies was assessed by Mann-Whitney U analysis (α=0.05). Unless otherwise stated, all data are presented as mean±standard error of the mean (S.E.M.).

Supplementary Figure Legends

Supplementary Figure S1. Conditional Ablation of DICER in the BM. A, Schematic representation of protocol for generation of Dicer$^{flox/flox}$/Cre^{ERT2} BMT chimera. Dicer$^{flox/flox}$ animals, were crossed with animals containing a single allele of Cre-ERT2, Cre$^{ERT2/-}$. Progeny that were homozygous for the Dicer^{flox} allele and heterozygous for the Cre-ERT2 allele, Dicer$^{flox/flox}$/Cre^{ERT2}, had their BM transplanted into lethally irradiated (1100rads) WT recipient animals. Following reconstitution, Dicer$^{flox/flox}$/Cre$^{ERT2/-}$ BMT animals were IP injected with 4-OHT every two days, beginning four days prior to implantation of LLCs. B, Growth rates of LLC in animals transplanted with Dicer$^{flox/flox}$/Cre$^{ERT2/-}$ BM (Mean±S.E.M, n=10), treated with 4-OHT, compared with animals transplanted with WT BM treated with 4-OHT. Controls include animals transplanted with Dicer$^{flox/flox}$/Cre$^{ERT2/-}$ BM and not treated with 4-OHT. Data analyzed by MANOVA (α=0.05, '*' P<0.05, '**' P<0.01). Right, tumor morphology at end point, Scale bar, 20mm. Similar trends were observed in repeat experiments. C, CD31^{+} immunostaining showing a lower vessel density in Dicer$^{flox/flox}$/Cre$^{ERT2/-}$ BMT LLC tumors treated with 4-OHT, compared with untreated Dicer$^{flox/flox}$/Cre$^{ERT2/-}$ BMT control (n=10 tumors/group, at least 5 fields each). Scale bar, 100μm. Data represented as average number of vessels per field±S.E.M. and analyzed by Unpaired t test (α=0.05).

Supplementary Figure S2. Retroviral Delivery of CRE-Recombinase. A, Schematic representation of the LV-Cre-ERT2 LV delivery vectors. The bisistronic cassette of GFP and Cre-ERT2 is separated by an IRES and driven by the Id1pr/p (Left) or EF_{long} (Right). The Self Inactivating (SIN) Long Terminal Repeats (LTRs) and the LoxP site in the LTR are shown. B Left, Murine ROSA26-lox-Stop-lox-LacZ 3T3 cells infected with Id1pr/p-Cre^{ERT2} and constitutive EF_{long}-CRE^{ERT2}, showing LacZ expression in both (arrows). Scale bar,

100μm. Right, similar numbers of $LacZ^+$ cells in Id1pr/p-Cre^{ERT2} and EF_{long}-CRE^{ERT2} with no expression in the negative control. These results show that the Id1pr/p-Cre^{ERT2} produces functional Cre-ERT2. C, Stable Id1pr/p-Cre^{ERT2} containing 293T clones (293T:Id1pr/p-Cre^{ERT2}) were treated with different concentrations of 4-OHT. Dose dependent self inactivation of the Id1pr/p-Cre^{ERT2} is indicated by a significant reduction in the number of GFP^+ cells as shown by microscopy in the left panel and FACS in the right panel (ANOVA, α=0.05).

Supplementary Figure S3. Analysis of $Dicer^{flox/flox}$:Id1pr/p-Cre^{ERT2} BMT animals. A, Schematic representation of the generation of $Dicer^{flox/flox}$:Id1pr/p-Cre^{ERT2} BMT and WT:Id1pr/p-Cre^{ERT2} BMT controls. BM extracted from WT or $Dicer^{flox/flox}$ animals was transduced with LV-Id1pr/p-Cre^{ERT2} and transplanted into WT animals. Following reconstitution, BMT animals were IP injected with 4-OHT, every two days, beginning four days prior to implantation of LLCs. B Upper, Representative FACS analysis of GFP^+ c-kit^+ BMDC from WT BMT, compared with WT:Id1pr/p-GFPIRES(I)Cre^{ERT2} BMT animals. Lower, high (63×) resolution image showing Dicer, GFP and Cre expression in c-kit^+ BMMNCs from $Dicer^{flox/flox}$:Id1pr/p-GFPICre^{ERT2} BMT animals. Scale bar 20μm. C, Image showing restricted expression of GFP and CRE^{ERT2} to VE-$Cadherin^+$ EPCs in LLC tumors grown in Id1pr/p-Cre^{ERT2} BMT animals. Scale bar, 20μm. D, Image of c-kit^+ BMMNCs, showing loss of DICER expression in VE-$Cadherin^+$ EPCs in $Dicer^{flox/flox}$:Id1pr/p-GFPCre^{ERT2} BMT 4-OHT treated animals (arrows), but not inWT:Id1pr/p-Cre^{ERT2} BMT mice. Scale bar, 50μm.

Supplementary Figure S4. Representative Scatter Plots of EPC Isolation and Analysis by FACS. A, PBMNCs were isolated and contaminating erythrocytes excluded by negative

selection for Ter119. Ter119^{-} cells were selected and CD11b^{+} cells removed. The c-kit^{+} fraction was identified, and separated into VE-Cadherin^{+} cells (and/or VEGFR2^{+} cells, *data not shown*), representing 0.05-0.1% of the c-kit^{+} fraction. B, BMMNCs were isolated and sorted into CD11b^{+} and CD11b^{-} fractions. From the CD11b^{-} fraction, VE-Cadherin^{+} cells were isolated. SSC-A denotes side scatter values, while FSC-A denotes forward scatter value. Data shown per 1×10^{5} cells.

Supplementary Figure S5. *ISH* Analysis of MiR-10b Expression in EPCs. A, High (63×) resolution image *ISH* of PBMNCs from tumor challenged (LLCs, Day 14) mice showing expression of miR-10b in c-kit^{+} VE-Cadherin^{+} CEPs. B, High (63×) resolution image *ISH* of BMMNCs from tumor challenged mice (LLC) showing hybridization of the positive control in VE-Cadherin^{+} EPCs and other BM cells, with no binding of the scrambled control. For A and B scale bar, 20μm. C, *ISH* of LLC tumor, showing hybridization of the positive control in EPCs and tumor cells, with no binding of the scrambled control. Scale bar, 40μM. D Upper, *ISH* of LLC tumor grown in C57BL/6 mice transplanted with BM from the Id1$^{+/GFP}$ reporter mouse, showing rhodamine-labeled miR-10b in Id1$^{+/GFP}$ EPCs (arrow) at the tumor-host boundary (dashed line). Scale bar, 100μM. Lower, high (63×) resolution image showing miR-10b in Id1$^{+/GFP}$ EPCs. E Upper, *ISH* of 4T1 tumor (Day 21) showing expression of miR-10b in VE-Cadherin^{+} EPCs at the tumor-stroma boundary (arrow). Scale bar, 100μM. Lower, high (63×) resolution image showing miR-10b in VE-Cadherin^{+} EPCs. F Upper, *ISH* of MDA-MB-231 tumor (Day 28) showing expression of miR-10b in VE-Cadherin^{+} EPCs at the tumor-stroma boundary (arrow). Scale bar, 100μM. Lower, high (63×) resolution image showing miR-10b in VE-Cadherin^{+} EPCs. Also shown in C-F, CD31^{+} vasculature.

Supplementary Figure S6. Analysis of MiR-10b and MiR-196b and HOXD10 in Dicer$^{flox/flox}$:Id1pr/p-Cre^{ERT2} BMT mice. A, *ISH* analysis showing reduced expression of miR-10b in VE-Cadherin^{+} EPCs from Dicer$^{flox/flox}$:Id1pr/p-Cre^{ERT2} BMT mice, treated with 4-OHT, compared with (*Lower*), WT: Id1pr/p-Cre^{ERT2} BMT mice treated with 4-OHT. Scale bar, 50μm. B & C Fluorescent microscopy showing increased HOXD10 expression in VE-Cadherin^{+} EPCs in the tumor-stroma of Dicer$^{flox/flox}$:Id1pr/p-Cre^{ERT2} BMT mice, compared with EPCs in the tumor-stroma of WT BMT and WT:Id1pr/p-Cre^{ERT2} BMT mice. Scale bar, 100μm. Also shown results of densitometry, represented as relative pixel density, subtracted from background±S.E.M. and analyzed by Unpaired *t* test (α=0.05, '*' P<0.05).

Supplementary Figure S7. MiRNA Expression in Tumor Vasculature using mCherry Exclusion. A Upper, Q-PCR analysis showing miRNA expression in CD11b^{-} CD31^{+} tumor vasculature with and without mCherry exclusion showing correlation between the two data sets (r2=9.158, by Pearson's), in particular miR-10b and miR-196b remained highly up-regulated in tumor vasculature. Data represented as mean (Log_2Fold)±S.E.M and analyzed by Unpaired *t* test (α=0.05, '*' P<0.05, '**' P<0.01). B, *ISH* of mCherry LLC tumors, showing miR-10b expression in mCherry^{-}CD31^{+} vasculature (box), and in mCherry^{+}CD31^{-} tumor cells (yellow arrow). Scale bar, 100μm.

Supplementary Figure S8. *ISH* Analysis of miR-10b Expression in Normal and Tumor Vasculature. A, *ISH* showing expression of miR-10b in CD31^{+} tumor vasculature in a 4T1 tumor (arrows). B, *ISH* showing expression of miR-10b in CD31^{+} tumor vasculature in MDA-MB-231 tumor (arrows). Scale bar, 50μm. C Upper, *ISH* of lung vasculature showing miR-10b is localized to CD11b^{+} cells (arrows). Scale bar, 100μm. Lower, high (63×) resolution image showing miR-10b in CD11b^{+} myeloid cells (white arrows), with little or no

expression of miR-10b in $CD31^+$ vasculature (yellow arrows). D, *ISH* showing no expression of miR-10b in $CD31^+$ dermal vasculature. Also shown hybridization of positive control (arrows) and no binding of scrambled control. Scale bar, 100μm.

Supplementary Figure S9. *ISH* Analysis of Normal and Tumor Vasculature; and Murine Endothelial Cells *In Vitro*. A, High (63×) resolution *ISH* image of LLC tumor showing cytoplasmic expression of miR-10b (white arrow, inset) as determined by F-actin and CD31 staining. Also shown miR-$10b^+$ $CD31^-$ cells undergoing division, marked by polarization of F-actin (yellow arrow). Scale bar, 50μm. B, *ISH* of Lung Vasculature Showing miR-451^+CD31^+ cells (arrow). Also shown hybridization of positive control and no binding of scrambled control. Scale bar, 100μm. C, *ISH* of murine endothelial cells showing expression of miR-10b and miR-196b (arrow). Also shown hybridization of positive control (arrow) and no binding of scrambled control. Scale bar,100μm.

Supplementary Figure S10. MiRNA Expression in Human Breast Tumor Endothelial Cells. A, *ISH* of IDC grade III tumor, showing miR-10b and miR-196bexpression in $CD31^+$ vasculature (arrows). Scale Bar, 100μm. B, *ISH* of DCIS tumor, showing no expression of miR-10b and miR-196b expression in $CD31^+$ vasculature. Scale Bar, 50μm. C, Scatter plot showing a significantly higher number of miR-$10b^+CD31^+$ vessels in IDC grade III tumors, compared with DCIS tumors. D, Scatter plot showing a significantly higher number of miR-$196b^+CD31^+$ vessels in IDC grade III tumors, compared with DCIS tumors. For C and D (α=0.05, by Mann Whitney U). E, *ISH* of human endothelial cells showing expression of tumor vascular miRNAs (arrow). Also shown, hybridization of positive control (arrow) and no binding of scrambled control. Scale bar, 100μM.

Supplementary Figure S11. Assessment of miRNA Suppression on the Function of Human and Murine Endothelial Cells. A, Representative image of human endothelial cells, transfected with labeled (Cy3, arrow) and unlabeled anti-miR grown either with or without Matrigel™. Scale bar, 100μm. B, Representative image of murine endothelial cells, transfected with labeled (Cy3, arrow) and unlabeled anti-miR, compared with transfection reagent only control (TC). Scale bar, 50μm. C Left, Representative image of anti-miR treated and non-treated murine and human endothelial cells, grown on Matrigel™, arrows indicate measurement of tube length. Scale bar, 100μm. Right, results of tube formation assay showing anti-miR treatment results in impaired tube length in murine and human endothelial cells, compared with TC and Scrambled Control (SC). Data is represented as mean tube length±S.E.M. D Left, Representative images of murine and human endothelial cells showing impaired wound healing in anti-miR treated cells compared with TC and SC. Scale bar, 100μm. Right, results of wound healing assay showing anti-miR treatment results in impaired migration rate in murine and human endothelial cells compared with TC and SC controls. Data is represented as mean % migration rate±S.E.M. E, Q-PCR analysis showing induction of miR-7 following miR-10b suppression in human (Log_2Fold 0.98±0.021) and murine (Log_2Fold 1.21±0.60) endothelial cells. Data is represented as mean % increase in expression±S.E.M. compared with SC. For C, D & E data is analyzed by Unpaired *t* test (α=0.05, '*' $P<0.05$, '**' $P<0.01$).

Supplementary Figure S12. RGD Peptide Directed Delivery of Anti-miRs using Liposomes. A, Scatter plot following FACS analysis of endothelial cells in culture treated with RGD-liposome-anti-miR *in vitro*, prior to administration. B, FACS analysis scatter plot of BM (upper) and peripheral blood (lower), from RGD-liposome-anti-miR injected, 4T1 tumor

implanted mice, showing uptake of FITC labeled anti-miR. C, Fluorescent microscopy of 4T1 tumor showing uptake of FITC labeled anti-miR in $CD31^+$ vasculature delivered using the RGD targeted liposomes. Scale bar, 50μm. D, FACS analysis bar graph (left) and fluorescent microscopy of BMMNCS cells (right), showing that 40-60% of c-$kit^+$$VEGFR2^+$ EPCs, from RGD-liposome-anti-miR treated 4T1 tumor implanted mice, having uptake of FITC labeled anti-miR. Scale bar, 20μM

Plummer_FigS1

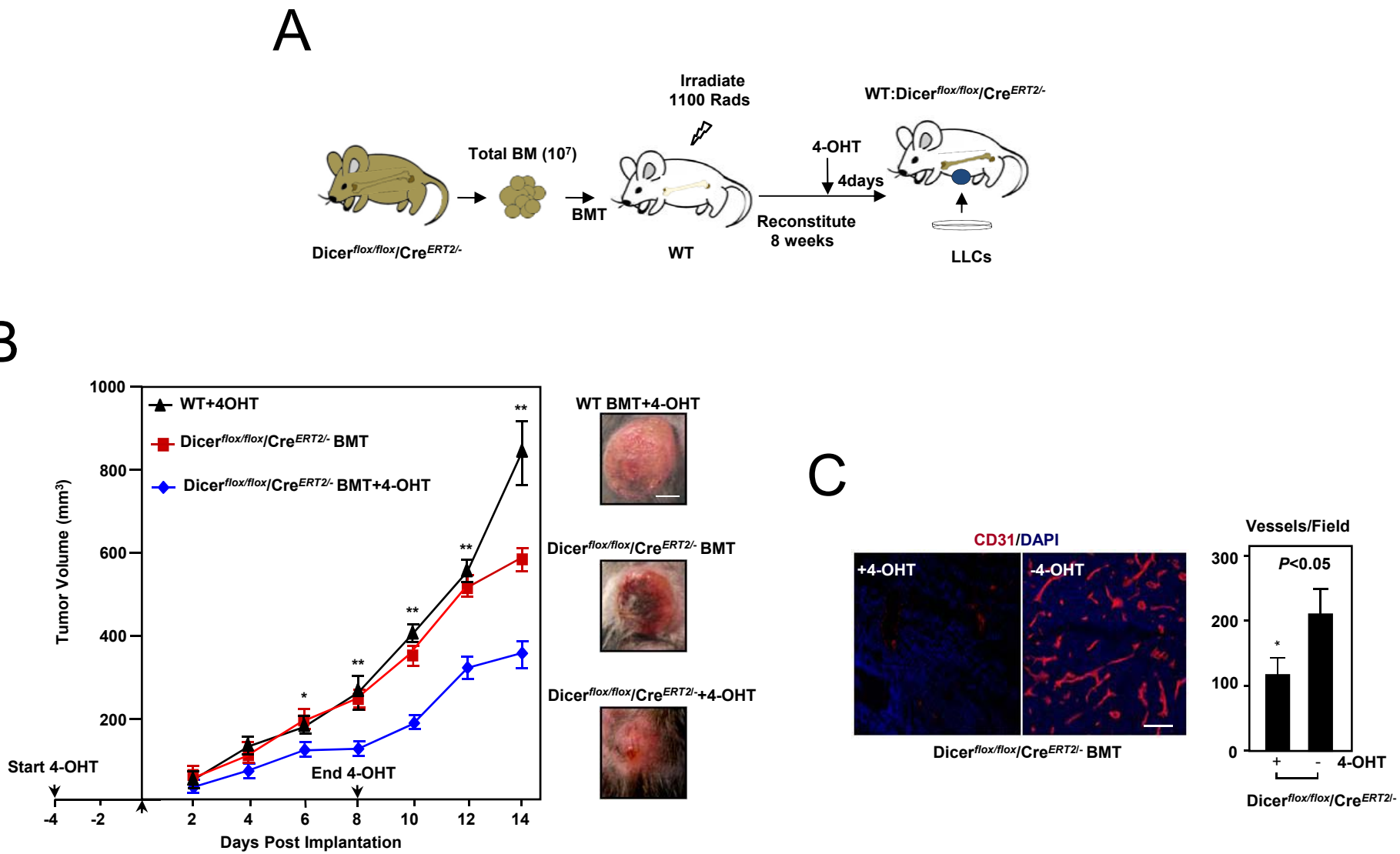

A

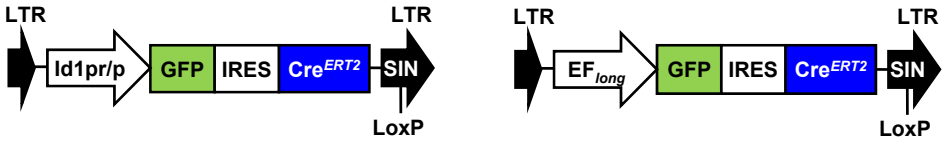
LTR
Id1pr/p
GFP
IRES
Cre^ERT2
SIN
LTR
LoxP
LTR
EF long
GFP
IRES
Cre^ERT2
SIN
LTR
LoxP

B

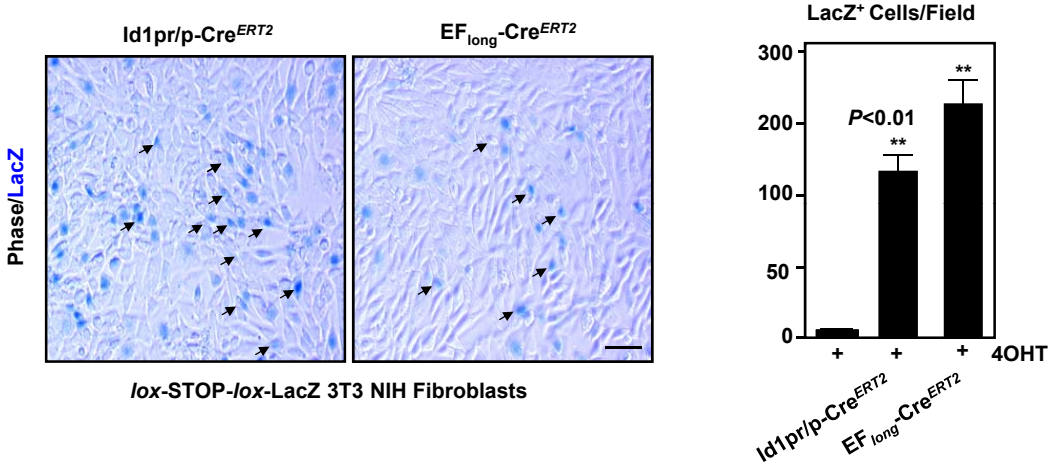
Id1pr/p-Cre^ERT2
EF long-Cre^ERT2
Phase/LacZ
lox-STOP-lox-LacZ 3T3 NIH Fibroblasts
LacZ+ Cells/Field
300
200
100
50
0
P<0.01
**
**
**
+
+
+
4OHT
Id1pr/p-Cre^ERT2
EF long-Cre^ERT2

C

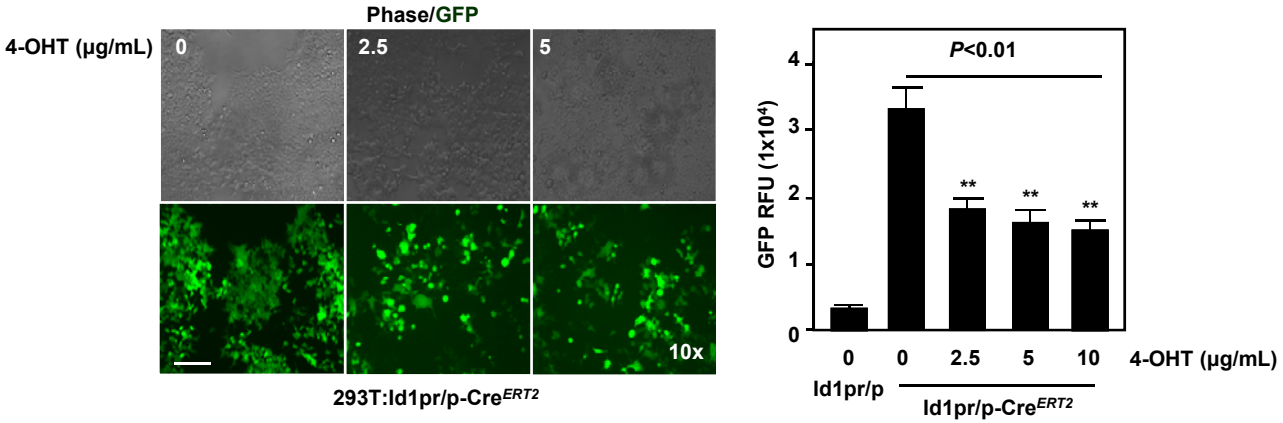
Phase/GFP
4-OHT (µg/mL)
0
2.5
5
10x
293T:Id1pr/p-Cre^ERT2
GFP RFU (1x10⁴)
4
3
2
1
0
P<0.01
**
**
**
0
0
2.5
5
10
4-OHT (µg/mL)
Id1pr/p
Id1pr/p-Cre^ERT2

A

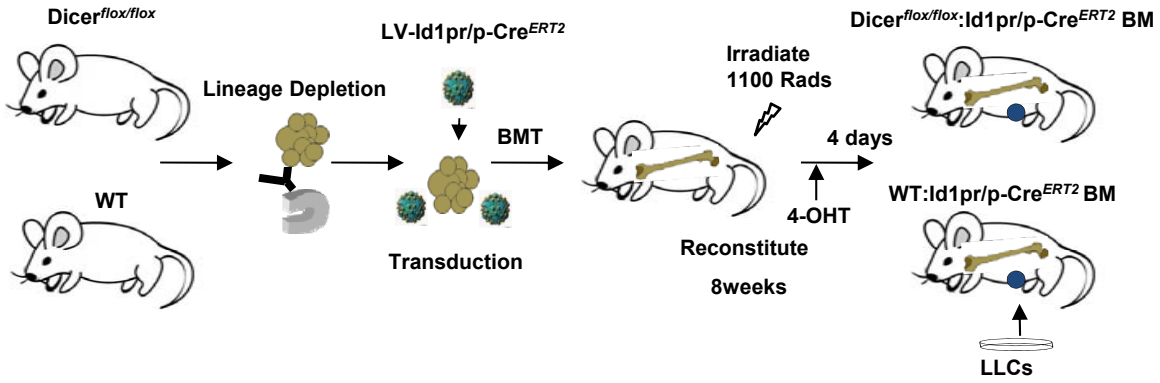

B

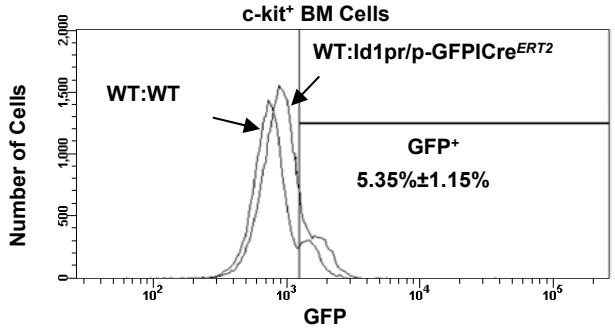

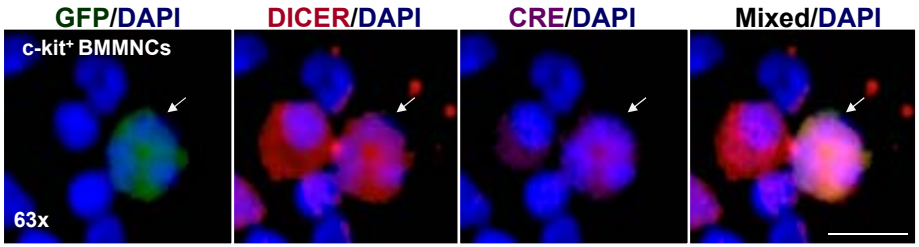

Dicer flox/flox :Id1pr/p-GFPICre ERT2

C

Dicer flox/flox :Id1pr/p-GFPICre ERT2

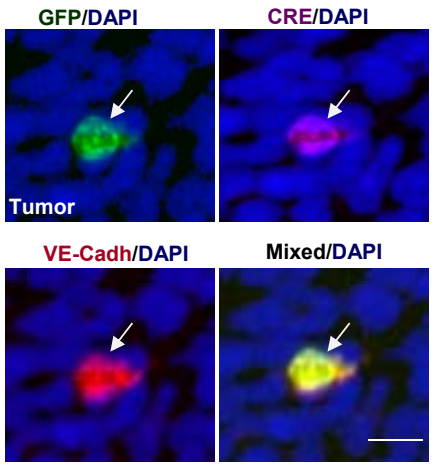

D

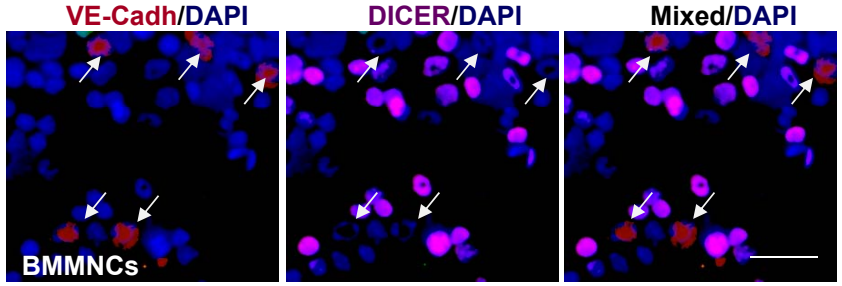

Dicer flox/flox :Id1pr/p-Cre ERT2

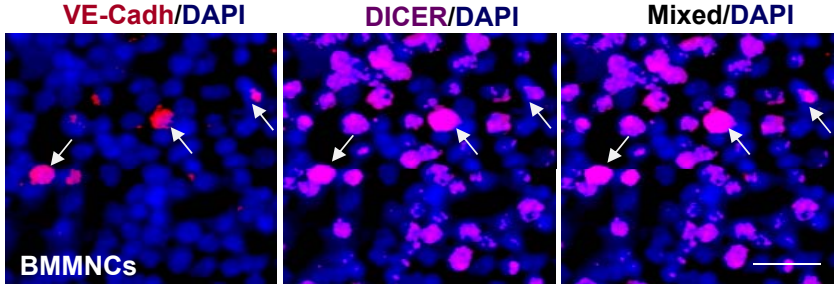

WT:Id1pr/p-Cre ERT2

Plummer_FigS4

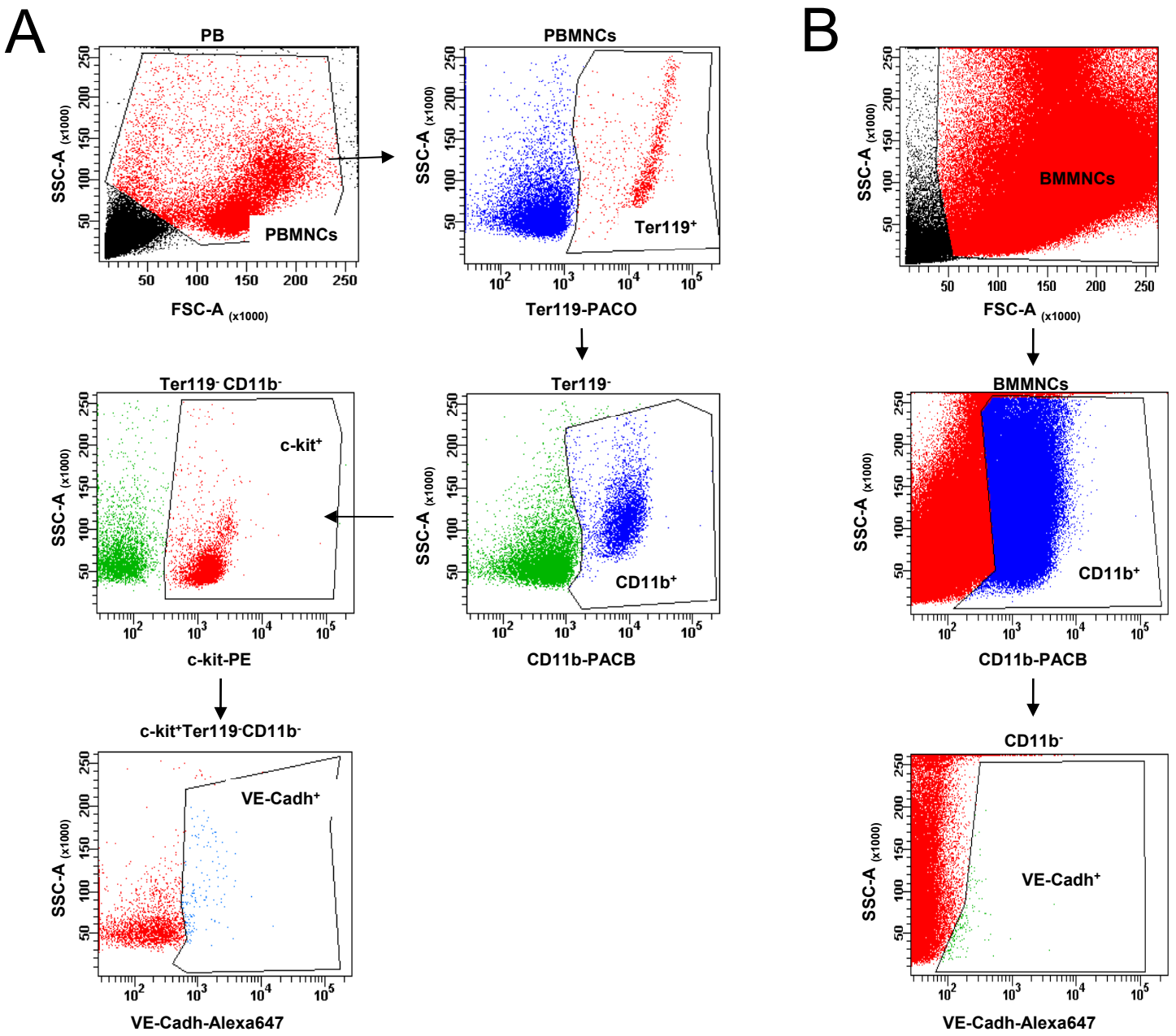

Plummer_FigS5

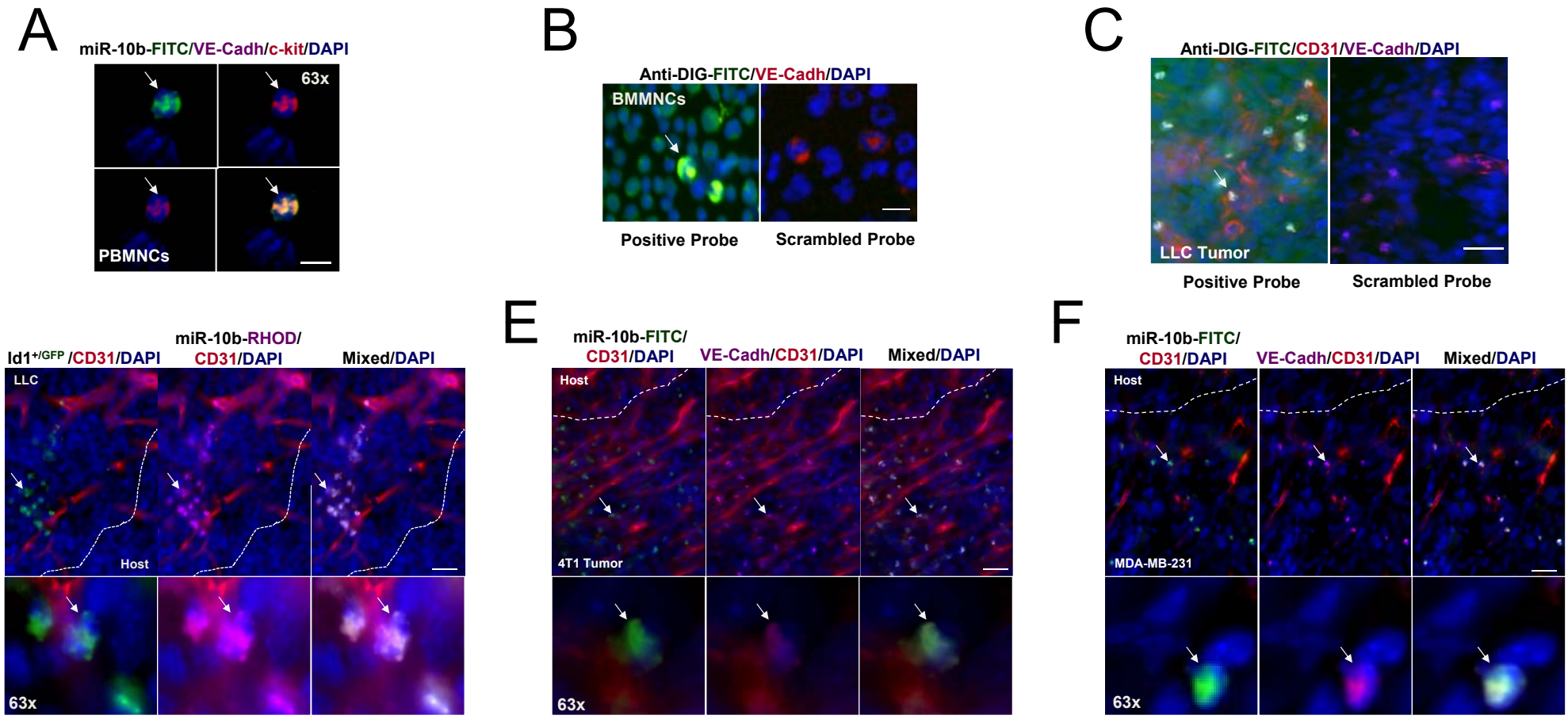

A

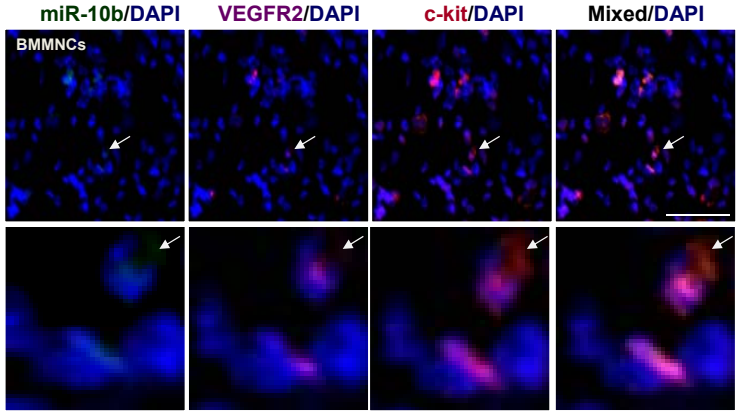

Dicer$^{flox/flox}$:Id1pr/p-Cre^{ERT2}

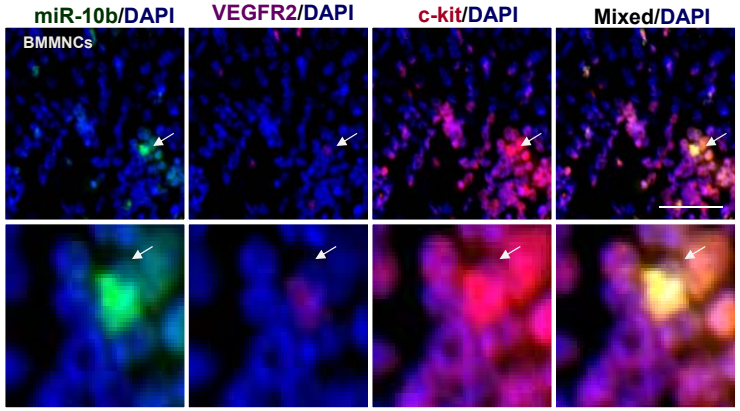

WT: Id1pr/p-Cre^{ERT2}

B

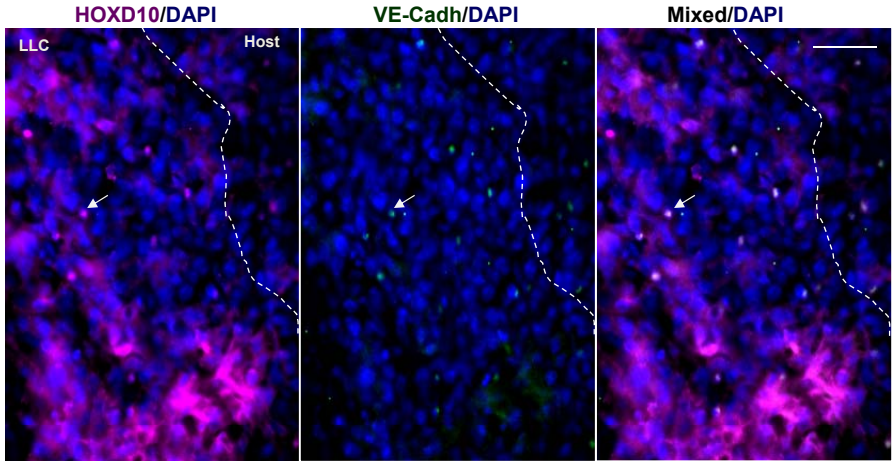

Dicer$^{flox/flox}$:Id1pr/p-Cre^{ERT2}

C

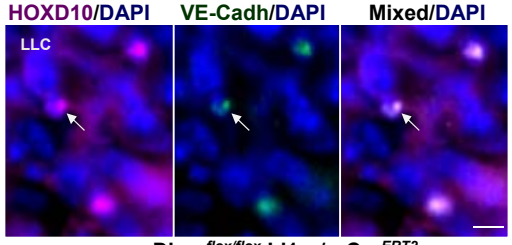

Dicer$^{flox/flox}$:Id1pr/p-Cre^{ERT2}

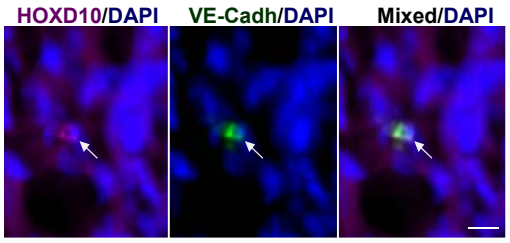

WT:Id1pr/p-Cre^{ERT2}

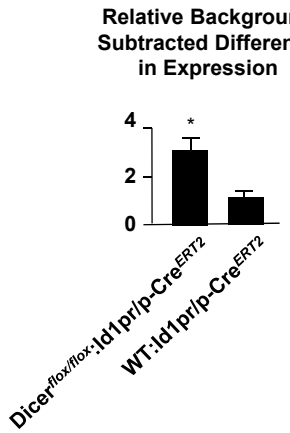

Plummer_FigS7

A

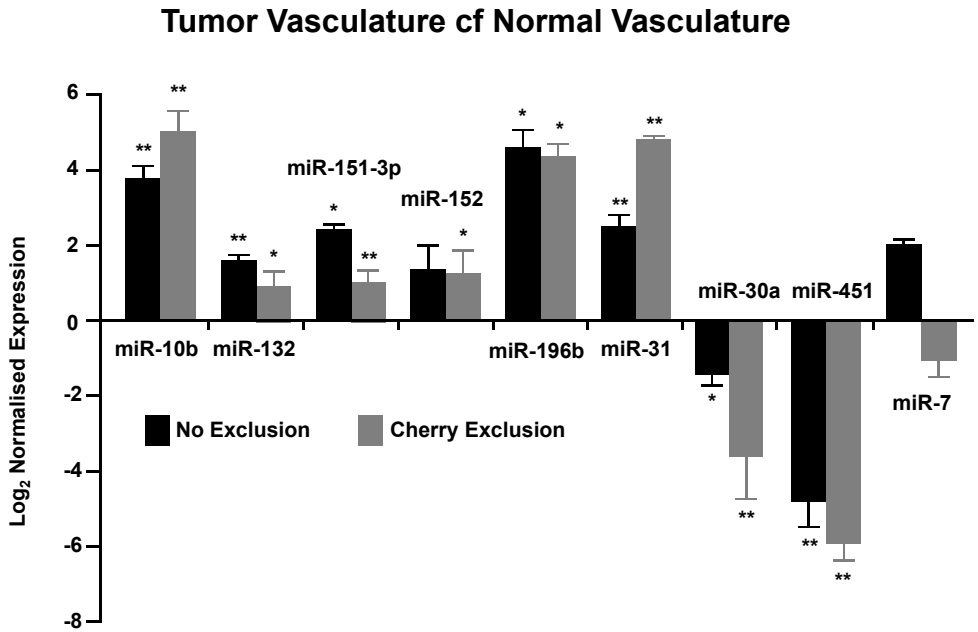

B

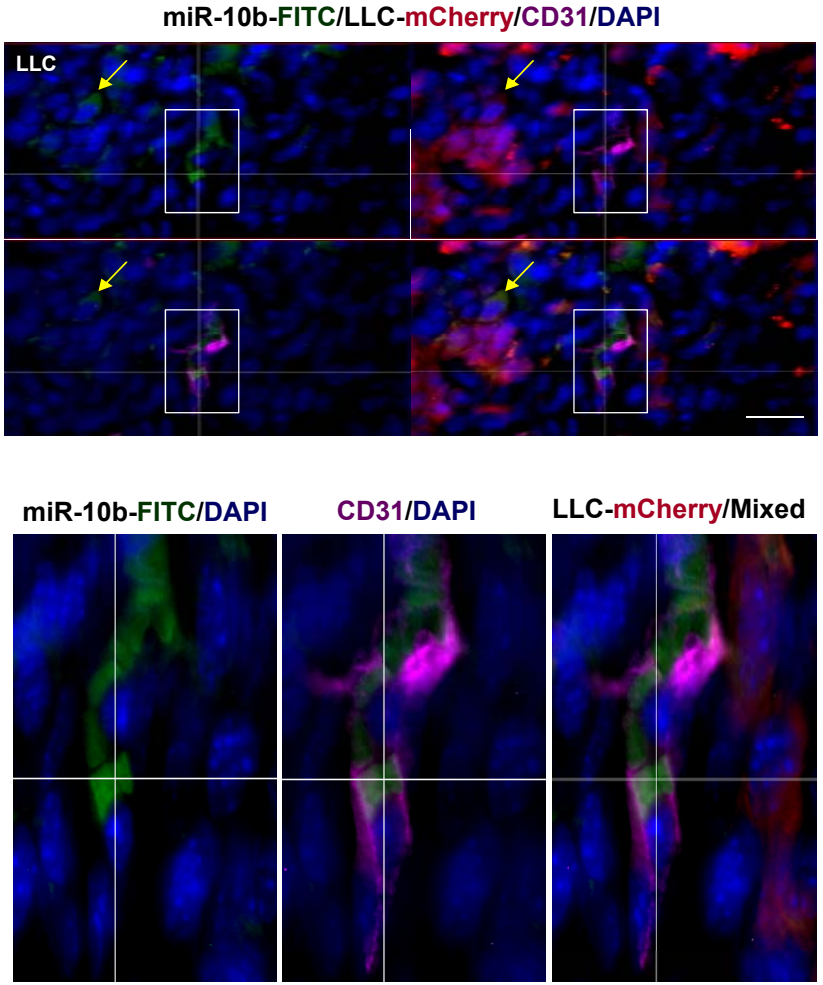

Plummer_FigS8

A

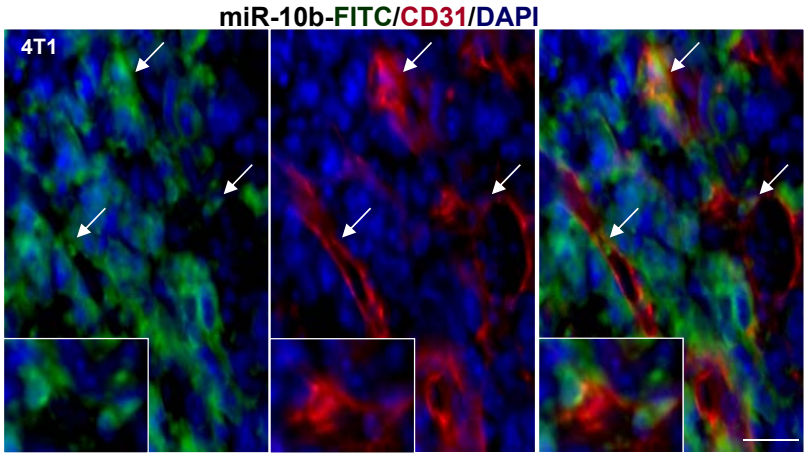

B

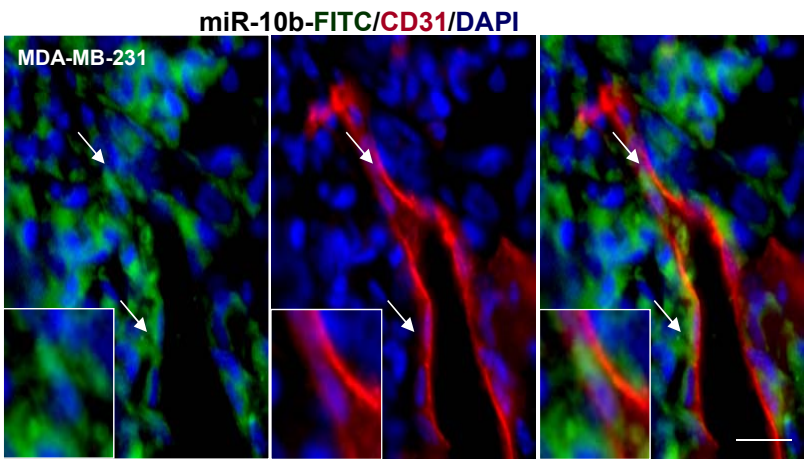

C

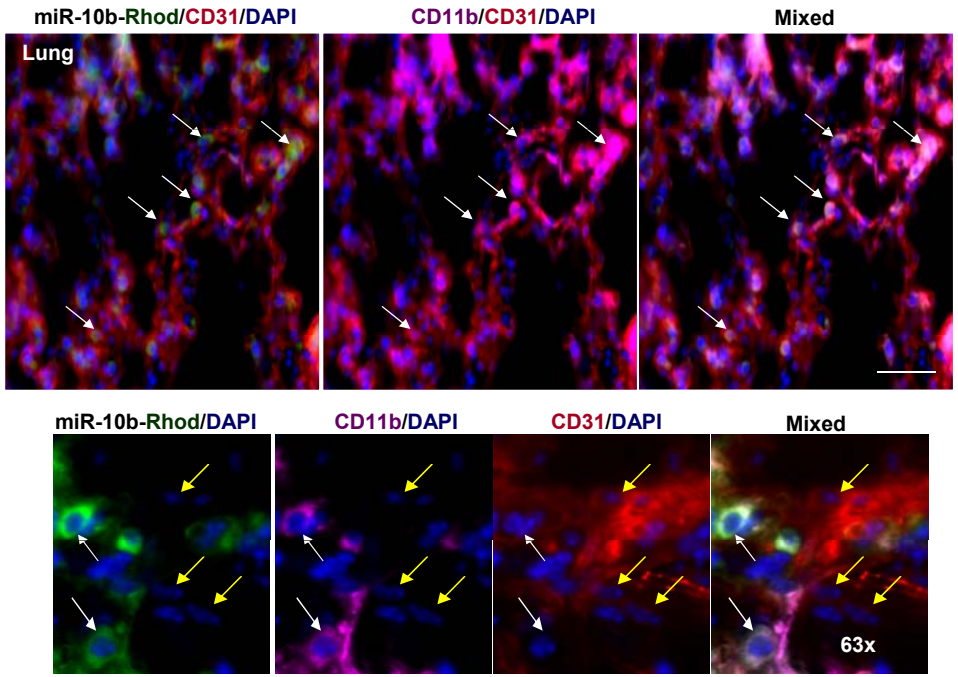

D

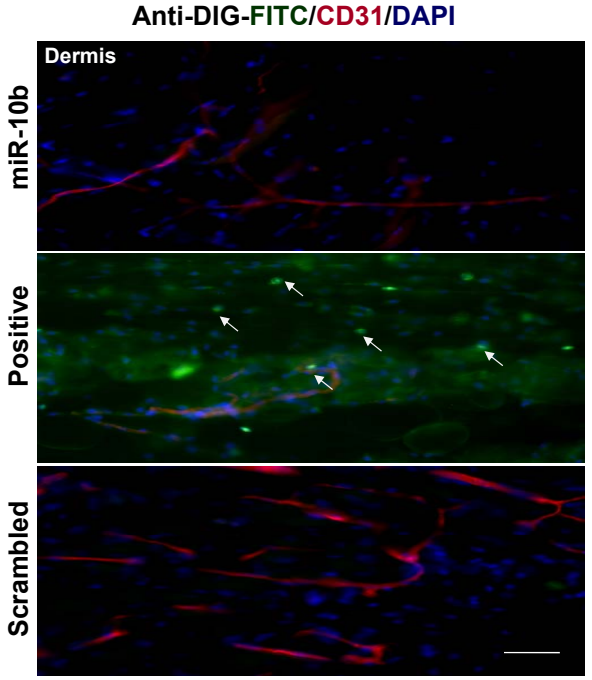

Plummer_FigS9

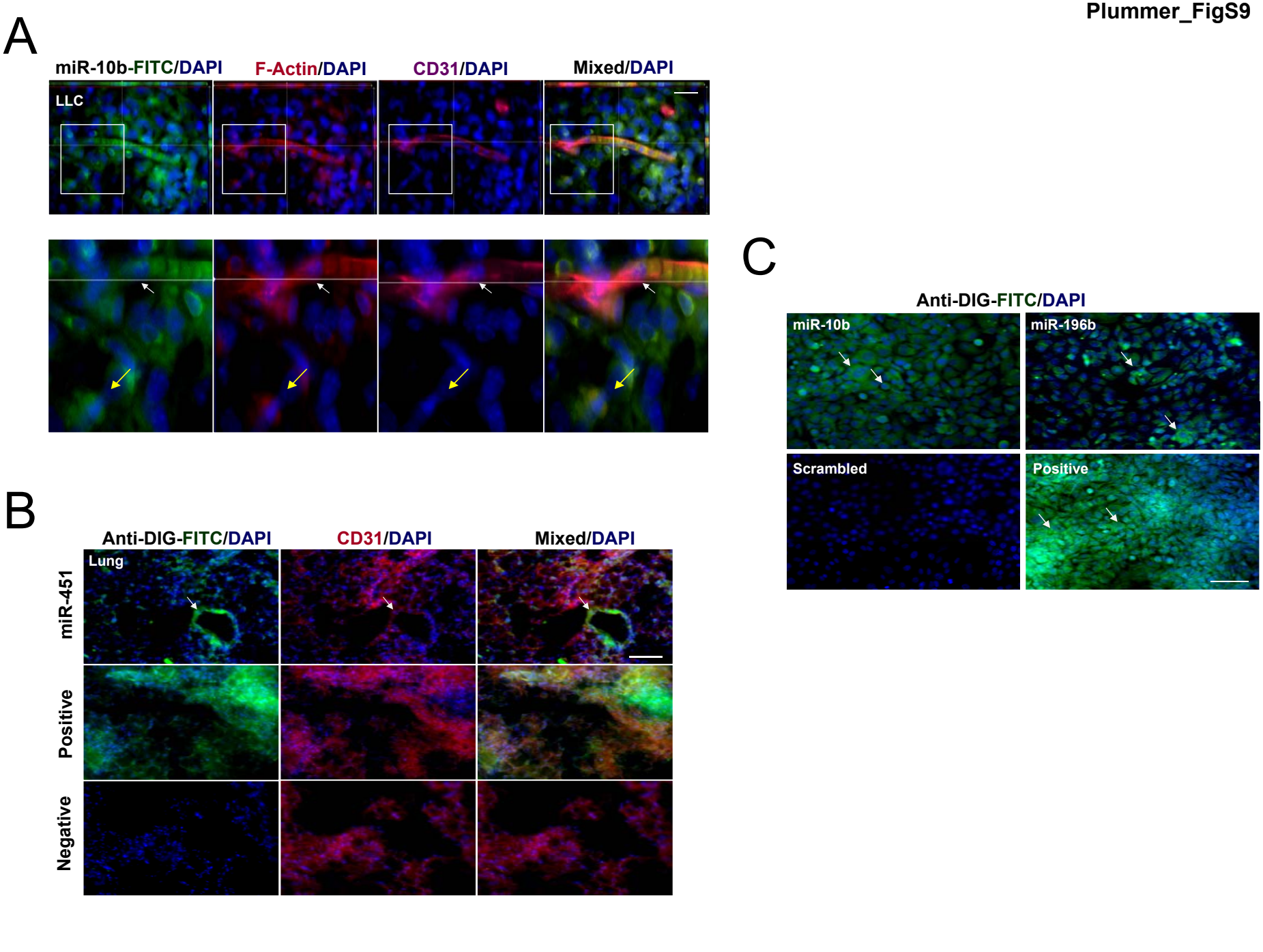

Plummer_FigS10

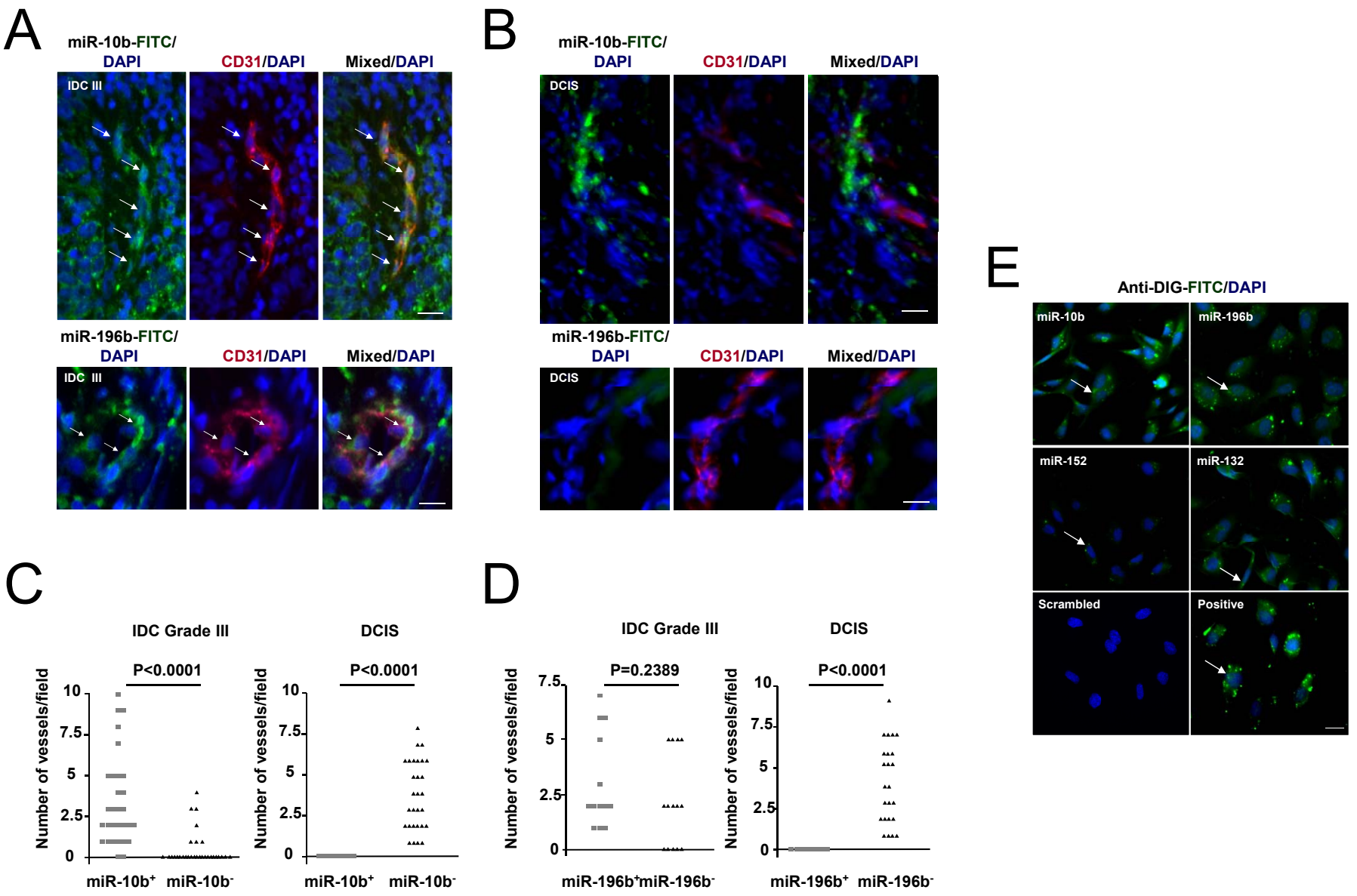

Plummer_FigS11

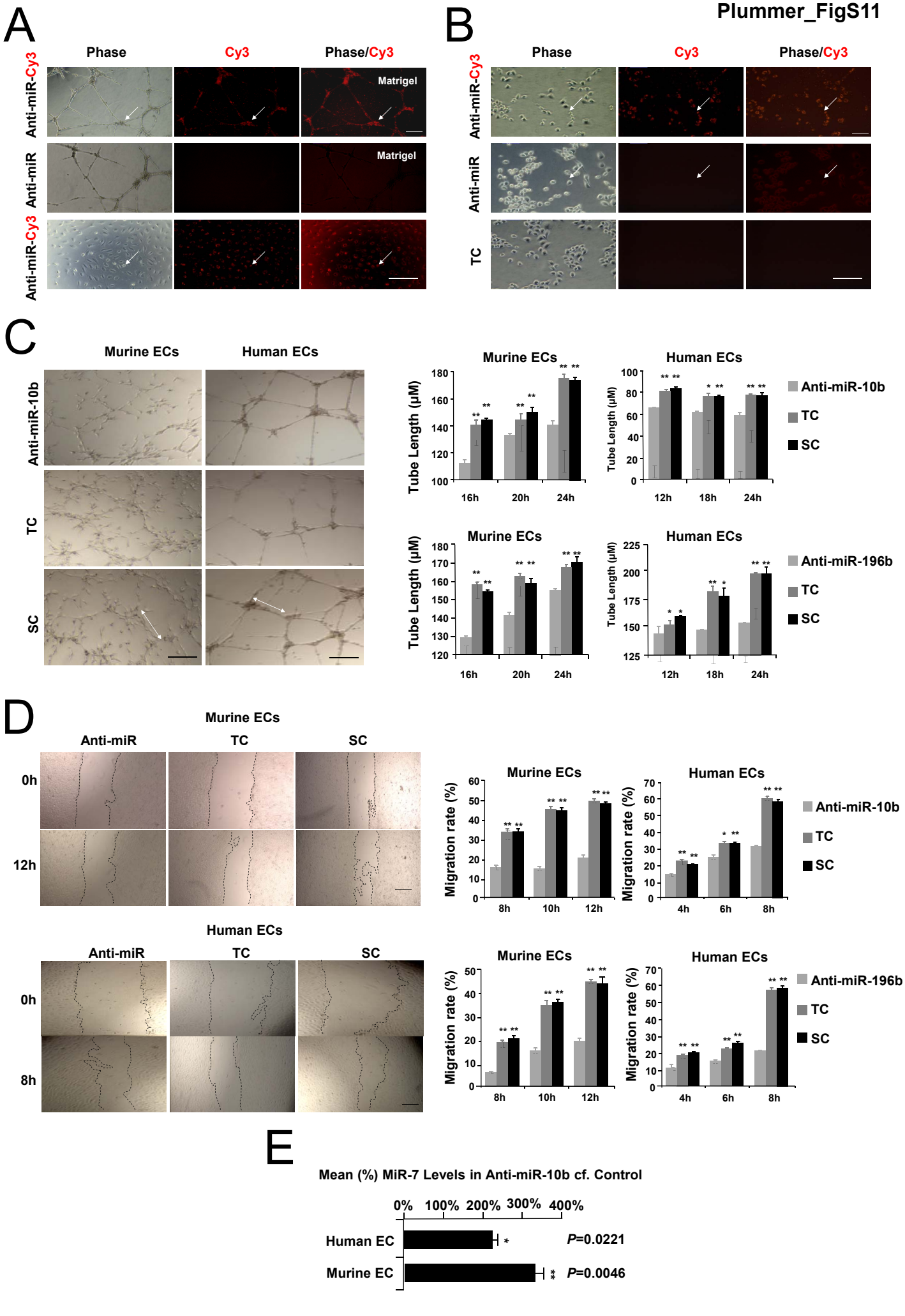

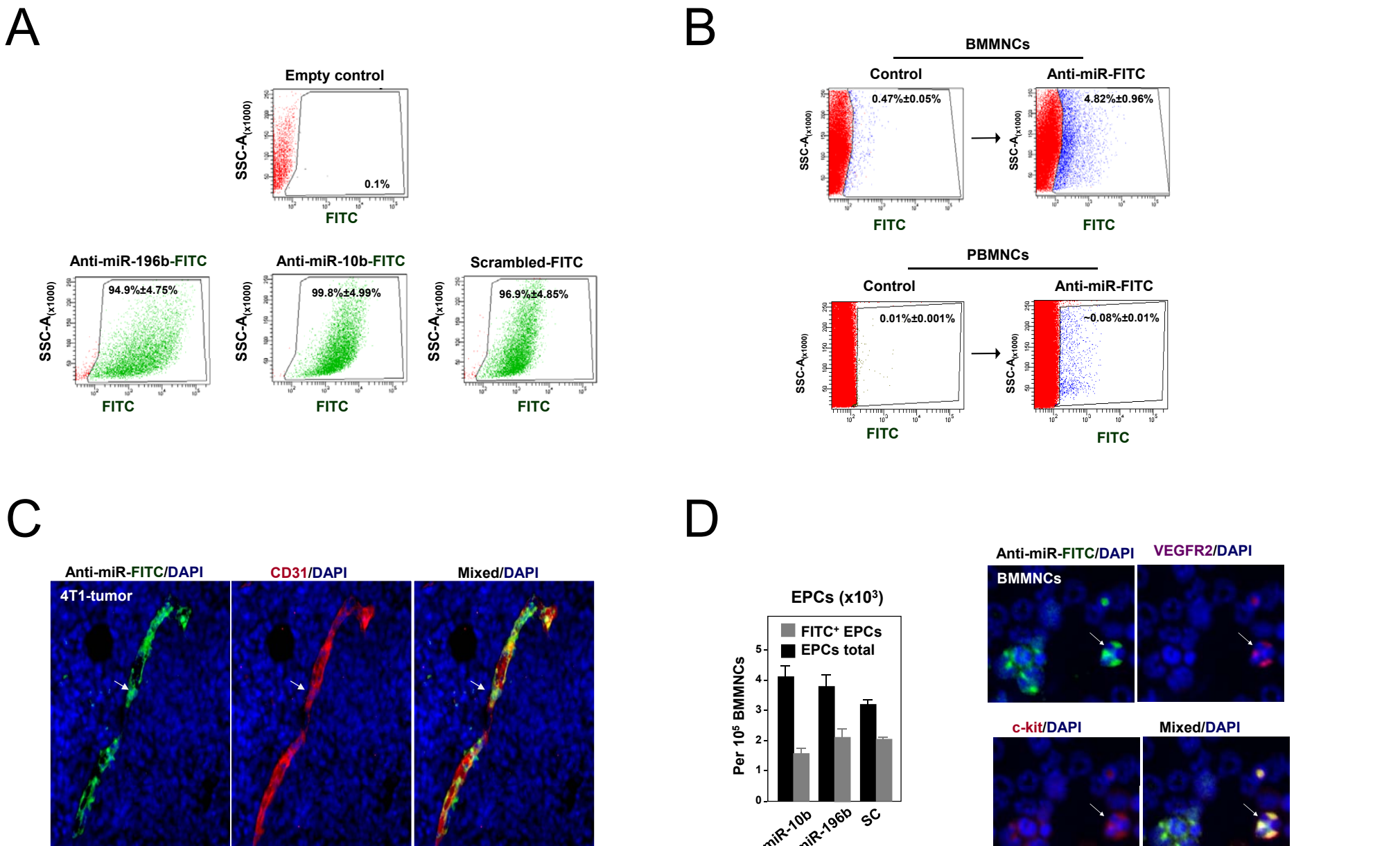
A
Empty control
SSC-A(x1000)
0.1%
FITC
Anti-miR-196b-FITC
94.9%±4.75%
Anti-miR-10b-FITC
99.8%±4.99%
Scrambled-FITC
96.9%±4.85%
B
BMMNCs
Control
Anti-miR-FITC
0.47%±0.05%
4.82%±0.96%
PBMNCs
0.01%±0.001%
~0.08%±0.01%
C
Anti-miR-FITC/DAPI
CD31/DAPI
Mixed/DAPI
4T1-tumor
D
EPCs (x10³)
FITC⁺ EPCs
EPCs total
Per 10⁵ BMMNCs
Anti-miR-10b
Anti-miR-196b
SC
Anti-miR-FITC/DAPI
VEGFR2/DAPI
BMMNCs
c-kit/DAPI
Mixed/DAPI

Table S1 EPCs cf Lineage Depleted Cells[#].

miR	Lin^{-}[†]	EPC[‡]	Fold
miR-18b	69.47	13.86	↓5.01
miR-29b	367.82	90.53	↓4.06
miR-33	58.99	14.89	↓3.96
miR-32	170.53	57.67	↓2.96
miR-125a-5p	52.06	17.97	↓2.90
miR-500	54.00	18.65	↓2.89
miR-17*	143.29	54.08	↓2.65
miR-30e	18318.90	6956.49	↓2.63
miR-128	307.21	117.74	↓2.61
miR-125b-5p	244.03	95.32	↓2.56
miR-16*	106.54	42.10	↓2.53
miR-101a	1272.20	519.38	↓2.45
miR-181a-1*	244.51	101.31	↓2.41
miR-181c	835.89	365.02	↓2.29
miR-872*	217.60	97.72	↓2.23
miR-181b	6861.00	3127.94	↓2.19
miR-450a-5p	216.31	99.26	↓2.18
miR-99a	201.48	94.46	↓2.13
miR-126-3p	975.15	470.61	↓2.07
miR-130b*	79.14	38.33	↓2.06
miR-181a	23798.10	11738.10	↓2.03
miR-181a-2*	59.96	29.78	↓2.01
miR-99b	354.92	177.98	↓1.99
miR-532-5p	289.48	146.32	↓1.98
miR-423-5p	359.27	184.31	↓1.95
miR-542-3p	387.48	206.04	↓1.88
miR-30d	19487.80	10376.60	↓1.88
miR-15b*	161.99	86.59	↓1.87
miR-203	416.17	223.16	↓1.86
miR-425*	121.05	65.03	↓1.86
miR-101b	4835.43	2652.02	↓1.82
miR-106b	3721.35	2046.39	↓1.82
miR-106a	199.38	110.55	↓1.80
miR-374	383.29	213.23	↓1.80
miR-146a	1018.18	567.47	↓1.79
miR-20b	581.86	324.47	↓1.79
miR-30a	2398.38	1340.13	↓1.79
miR-126-5p	189.39	106.27	↓1.78
miR-363	55.45	31.15	↓1.78
miR-18a	1364.88	767.18	↓1.78

miR	Lin^{-}	EPC	Fold
Let-7b	1217.56	705.40	↓1.73
Let-7d*	208.09	120.82	↓1.72
miR-150	576.38	340.72	↓1.69
miR-181d	1411.79	836.83	↓1.69
miR-301a	52.22	30.97	↓1.69
miR-345-5p	51.74	31.32	↓1.65
miR-185	109.76	66.91	↓1.64
miR-27b	2221.56	1357.93	↓1.64
miR-27a	1612.46	992.73	↓1.62
miR-15a	972.57	601.01	↓1.62
miR-196b	1698.53	1066.15	↓1.59
miR-21	45556.20	28608.40	↓1.59
miR-423-3p	418.59	263.20	↓1.59
miR-142-3p	35128.90	22267.30	↓1.58
miR-1839-5p	339.29	215.28	↓1.58
miR-24-2*	141.20	91.04	↓1.55
miR-30b	654.88	423.89	↓1.54
miR-29a	2881.92	1886.55	↓1.53
miR-19a	151.51	101.31	↓1.50
Let-7c	18412.40	12382.20	↓1.49
miR-19b	1255.76	861.13	↓1.46
miR-20a	8656.23	6015.96	↓1.44
miR-484	131.20	91.21	↓1.44
miR-93	14044.20	10007.90	↓1.40
miR-503	59.96	42.78	↓1.40
miR-92a	7189.97	5140.79	↓1.40
miR-1944	240.16	172.16	↓1.40
Let-7a	41392.00	29880.80	↓1.39
miR-139-3p	99.13	72.05	↓1.38
Let-7d	1936.75	1415.43	↓1.37
miR-221	535.77	391.89	↓1.37
miR-106b*	205.02	150.08	↓1.37
miR-28	73.02	53.74	↓1.36
miR-361	75.92	56.13	↓1.35
miR-340-3p	82.69	61.61	↓1.34
miR-451	5114.92	3820.85	↓1.34
miR-107	65.12	51.68	↓1.26
miR-222	301.89	240.10	↓1.26
miR-30c	4968.09	3989.42	↓1.25
miR-23b	421.49	338.84	↓1.24

miR	Lin^{-}	EPC	Fold
miR-425	3079.20	2522.99	↓1.22
miR-155	232.75	196.29	↓1.19
miR-744	1284.13	1089.94	↓1.18
miR-362-5p	110.89	95.32	↓1.16
miR-17	3891.56	3354.01	↓1.16
miR-652	232.58	201.76	↓1.15
miR-342-3p	189.71	168.22	↓1.13
miR-10a	9280.49	8300.22	↓1.12
miR-139-5p	303.18	271.24	↓1.12
Let-7i	2058.44	1872.35	↓1.10
miR-140*	13132.60	11955.90	↓1.10
miR-28*	230.81	210.49	↓1.10
miR-25	1880.02	1760.77	↓1.07
miR-194	347.83	326.01	↓1.07
miR-186	1610.04	1514.86	↓1.06
miR-22	135.39	128.69	↓1.05
miR-192	625.87	615.05	↓1.02
miR-151-3p	188.90	187.39	↓1.01
miR-322	501.60	503.47	↑1.00
miR-872	527.06	531.02	↑1.01
miR-103	7924.31	7991.84	↑1.01
miR-98	282.07	287.16	↑1.02
miR-130a	97.68	99.60	↑1.02
Let-7f	81353.90	83690.10	↑1.03
miR-23a	809.29	836.15	↑1.03
miR-148a*	98.97	105.42	↑1.07
miR-191	7842.59	8434.73	↑1.08
miR-130b	430.68	477.12	↑1.11
miR-345-3p	62.54	70.85	↑1.13
miR-223	3504.24	4223.53	↑1.21
miR-15b	813.64	996.84	↑1.23
miR-149	120.40	154.36	↑1.28
miR-142-5p	1344.25	1728.94	↑1.29
miR-140	556.08	756.06	↑1.36
miR-301b	76.24	104.22	↑1.37
miR-200c	128.78	181.23	↑1.41
miR-26b	742.56	1045.44	↑1.41
miR-339-3p	62.54	91.21	↑1.46
miR-26a	4975.18	7517.12	↑1.51
miR-1981	287.39	446.48	↑1.55

miR	Lin^{-}	EPC	Fold
Let-7g	8860.77	13879.80	↑1.57
miR-27a*	83.81	133.14	↑1.59
miR-148b	503.85	801.75	↑1.59
miR-2133	462.59	741.68	↑1.60
miR-24	11083.10	18193.20	↑1.64
miR-338-5p	37.39	64.17	↑1.72
miR-27b*	88.49	162.06	↑1.83
miR-152	100.58	188.93	↑1.88
miR-148a	6909.84	12998.50	↑1.88
miR-340-5p	317.53	605.98	↑1.91
miR-16	5278.68	10313.60	↑1.95
miR-30a*	74.95	157.61	↑2.10
miR-378	29544.30	75826.50	↑2.57
miR-7a	327.04	852.58	↑2.61
miR-30e*	678.25	1948.85	↑2.87
miR-143	55.29	379.40	↑6.86
miR-1	6.45	108.16	↑16.78

[†]Lin^{-}, Lineage depleted cells; [‡]EPC, Endothelial Progenitor Cells.

[#]Correlation by Pearson's r^2=0.7836.

Table S2 EPCs cf Myeloid Progenitors[#].

miR	MP[†]	EPC[‡]	Fold	*miR*	MP	EPC	Fold	*miR*	MP	EPC	Fold	*miR*	MP	EPC	Fold
miR-423-5p	774.35	184.31	↓4.20	**miR-27a**	1755.95	992.73	↓1.77	**miR-142-5p**	2084.45	1728.94	↓1.21	**miR-130b**	315.33	477.12	↑1.51
Let-7b	2485.60	705.40	↓3.52	**miR-23a**	1432.96	836.15	↓1.71	**miR-126-3p**	556.41	470.61	↓1.18	**miR-451**	2314.14	3820.85	↑1.65
miR-338-3p	100.78	30.80	↓3.27	**miR-744**	1833.76	1089.94	↓1.68	**miR-322**	589.17	503.47	↓1.17	**miR-16**	5979.34	10313.60	↑1.72
miR-149	501.04	154.36	↓3.25	**miR-125b-5p**	159.54	95.32	↓1.67	**miR-221**	454.57	391.89	↓1.16	**miR-130a**	50.21	99.60	↑1.98
miR-338-5p	198.17	64.17	↓3.09	**miR-106b**	3424.29	2046.39	↓1.67	**miR-20b**	374.80	324.47	↓1.16	**miR-152**	92.05	188.93	↑2.05
miR-135a*	66.77	22.59	↓2.96	**miR-15b***	142.98	86.59	↓1.65	**miR-155**	223.99	196.29	↓1.14	**miR-7a**	410.77	852.58	↑2.08
miR-223	12074.60	4223.53	↓2.86	**miR-345-5p**	50.92	31.32	↓1.63	**miR-99b**	200.66	177.98	↓1.13	**miR-30e***	922.31	1948.85	↑2.11
miR-1839-5p	601.82	215.28	↓2.80	**miR-374**	345.24	213.23	↓1.62	**miR-484**	100.78	91.21	↓1.10	**miR-30a***	73.00	157.61	↑2.16
miR-139-3p	194.79	72.05	↓2.70	**miR-181c**	589.53	365.02	↓1.62	**miR-148a***	116.27	105.42	↓1.10	**miR-27a***	54.66	133.14	↑2.44
miR-29b	238.23	90.53	↓2.63	**miR-1944**	275.98	172.16	↓1.60	**miR-92a**	5658.13	5140.79	↓1.10	**miR-2133**	301.98	741.68	↑2.46
miR-17*	141.20	54.08	↓2.61	**miR-181a**	18688.00	11738.10	↓1.59	**miR-107**	56.26	51.68	↓1.09	**miR-151-3p**	75.85	187.39	↑2.47
miR-192	1575.94	615.05	↓2.56	**miR-32**	90.63	57.67	↓1.57	**miR-128**	126.95	117.74	↓1.08	**miR-27b***	61.25	162.06	↑2.65
miR-542-3p	490.00	206.04	↓2.38	**miR-532-5p**	229.69	146.32	↓1.57	**miR-340-5p**	649.89	605.98	↓1.07	**miR-1**	29.56	108.16	↑3.66
Let-7c	28660.80	12382.20	↓2.31	**miR-181d**	1302.63	836.83	↓1.56	**miR-222**	257.11	240.10	↓1.07	**miR-378**	17491.30	75826.50	↑4.34
miR-181a-1*	232.00	101.31	↓2.29	**miR-27b**	2088.01	1357.93	↓1.54	**miR-98**	307.32	287.16	↓1.07	**miR-143**	58.94	379.40	↑6.44
miR-194	745.86	326.01	↓2.29	**miR-425***	99.89	65.03	↓1.54	**miR-26b**	1039.65	1045.44	↑1.01				
miR-423-3p	592.20	263.20	↓2.25	**miR-146a**	864.98	567.47	↓1.52	**miR-21**	27803.30	28608.40	↑1.03				
miR-101a	1153.42	519.38	↓2.22	**miR-101b**	3984.09	2652.02	↓1.50	**miR-15b**	965.40	996.84	↑1.03				
miR-340-3p	134.43	61.61	↓2.18	**miR-872***	145.65	97.72	↓1.49	**miR-196b**	1007.95	1066.15	↑1.06				
miR-139-5p	590.42	271.24	↓2.18	**miR-18a**	1126.89	767.18	↓1.47	**miR-342-3p**	158.29	168.22	↑1.06				
miR-30e	15048.10	6956.49	↓2.16	**miR-130b***	56.26	38.33	↓1.47	**miR-425**	2333.90	2522.99	↑1.08				
miR-30d	22143.80	10376.60	↓2.13	**miR-200c**	253.37	181.23	↓1.40	**miR-106a**	100.42	110.55	↑1.10				
miR-181b	6663.24	3127.94	↓2.13	**miR-362-5p**	132.65	95.32	↓1.39	**miR-17**	3043.98	3354.01	↑1.10				
miR-181a-2*	61.43	29.78	↓2.06	**miR-22**	178.05	128.69	↓1.38	**miR-25**	1591.07	1760.77	↑1.11				
miR-24-2*	187.13	91.04	↓2.06	**miR-30c**	5395.15	3989.42	↓1.35	**miR-345-3p**	63.39	70.85	↑1.12				
miR-450a-5p	202.45	99.26	↓2.04	**miR-150**	458.84	340.72	↓1.35	**miR-140**	670.19	756.06	↑1.13				
miR-10a	16747.20	8300.22	↓2.02	**miR-23b**	455.46	338.84	↓1.34	**Let-7f**	73691.90	83690.10	↑1.14				
miR-652	403.11	201.76	↓2.00	**miR-19a**	133.54	101.31	↓1.32	**miR-191**	7084.86	8434.73	↑1.19				
miR-185	133.36	66.91	↓1.99	**miR-140***	15686.70	11955.90	↓1.31	**Let-7i**	1568.99	1872.35	↑1.19				
miR-135a	51.28	25.84	↓1.98	**miR-29a**	2446.08	1886.55	↓1.30	**miR-186**	1220.19	1514.86	↑1.24				
miR-582-3p	50.39	25.50	↓1.98	**miR-148a**	16664.40	12998.50	↓1.28	**miR-126-5p**	85.46	106.27	↑1.24				
miR-142-3p	42939.40	22267.30	↓1.93	**miR-19b**	1101.61	861.13	↓1.28	**miR-24**	14406.00	18193.20	↑1.26				
miR-16*	79.41	42.10	↓1.89	**miR-103**	10219.50	7991.84	↓1.28	**miR-872**	419.31	531.02	↑1.27				
Let-7a	55970.10	29880.80	↓1.87	**miR-106b***	189.27	150.08	↓1.26	**miR-28***	165.59	210.49	↑1.27				
miR-203	412.90	223.16	↓1.85	**miR-30a**	1674.58	1340.13	↓1.25	**miR-28**	41.31	53.74	↑1.30				
miR-93	18302.30	10007.90	↓1.83	**Let7d***	150.81	120.82	↓1.25	**miR-339-3p**	69.44	91.21	↑1.31				
miR-15a	1090.57	601.01	↓1.81	**miR-148b**	997.45	801.75	↓1.24	**Let-7g**	10290.20	13879.80	↑1.35				
miR-503	77.27	42.78	↓1.81	**miR-99a**	115.73	94.46	↓1.23	**miR-1981**	311.77	446.48	↑1.43				
miR-361	99.53	56.13	↓1.77	**miR-20a**	7325.77	6015.96	↓1.22	**miR-26a**	5062.37	7517.12	↑1.48				
miR-30b	750.67	423.89	↓1.77	**Let7d**	1713.39	1415.43	↓1.21	**miR-301b**	68.91	104.22	↑1.51				

[†]MP, Myeloid Progenitors; [‡]EPC, Endothelial Progenitor Cell

[#]Correlation by Pearsons r^2=0.6672.

Table S3 Small RNAs Regulated in Response to Tumor.

	Endothelial Progenitor Cells		Myeloid Progenitor Cells		Lineage (Stem) Depleted Cells	
	Log_2Fold	**P_{value}**	**Log_2Fold**	**P_{value}**	**Log_2Fold**	**P_{value}**
miR-30b	↓ 4.84±0.0898	<0.0001**	↓ 0.58±0.1796	0.0848	↑1.69±0.0817	0.0176*
miR-126-3p	↓ 4.09±0.0714	<0.0001**	↑ 0.47±0.0959	0.0027	↑1.61±0.0204	<0.0001**
miR-126-5p	↓ 3.68±0.2756	<0.0001**	↑ 0.03±0.3327	0.9368	↑0.57±0.0551	0.0208*
miR-20a	↓ 3.59±0.2041	<0.0001**	↓ 0.45±0.0714	0.0318*	↑2.84±0.0286	<0.0001**
miR-17-5p	↓ 3.36±0.1061	<0.0001**	↓ 1.14±0.0817	<0.0001**	↑3.10±0.0531	<0.0001**
miR-29a	↓ 2.97±0.1551	<0.0001**	↓ 0.59±0.161258	0.0106	↑3.06±0.0857	<0.0001**
miR-31	↓ 2.70±0.2878	0.0262*	↑ 0.11±0.3475	0.7998	↑0.97±0.4578	0.1317
miR-181a	↓ 2.18±0.1633	<0.0001**	↓ 0.37±0.0102	0.1054	↑3.57±0.0347	<0.0001**
miR-130a	↓ 1.18±0.0102	<0.0001**	NED	-	↑3.06±0.1327	<0.0001**
miR-222	↓ 0.02±0.0855	0.8915	↓ 0.13±0.3377	0.7213	↑0.61±0.1072	0.0792
Let-7b	↑ 0.23±0.0694	0.0265*	↓ 0.51±0.0551	<0.0001**	↑1.23±0.0980	0.0002**
miR-30a*	↑ 0.25±0.2593	0.5630	↓ 2.53±0.2246	0.0070**	↑1.52±0.2518	0.0031*
miR-106a	↑ 0.29±0.2409	0.2755	↑ 0.05±0.0674	0.8222	↑0.57±0.0694	0.0365*
miR-378	↑ 0.39±0.3103	0.2669	↑ 0.69±0.5083	0.2271	↓2.42±0.1347	<0.0001**
miR-15b	↑ 0.40±0.1245	0.0350*	↓ 1.43±0.2552	0.0015*	↑1.07±0.0775	0.0070*
Let-7i	↑ 0.45±0.1143	0.0986	↓ 1.74±0.2102	0.0002**	↑1.43±0.1796	0.0020**
Let-7d	↑ 0.48±0.1531	0.7011	↓ 0.675±0.1368	0.0033	↑1.9±0.0735	<0.0001**
Let-7g	↑ 0.69±0.2919	0.1456	↓ 4.95±0.3470	<0.0001**	↑9.5±0.3184	<0.0001**
miR-221	↑ 0.93±0.0707	0.0002**	↓ 0.32±0.2674	0.3964	↑1.30±0.0184	<0.0001**
miR-196b	↑ 1.46±0.2995	0.0148*	↑ 1.99±0.7217	0.0321*	↓2.39±0.1563	0.0012**
miR-7	↑ 1.62±0.0751	0.0111*	↓ 1.48±0.6364	0.0147*	↑1.36±0.0782	0.9212
Let-7a	↑ 1.79±0.0980	<0.0001**	↓ 1.84±0.2735	0.0010**	↑2.145±0.0163	<0.0001**
miR-151	↑ 1.86±0.2044	0.0305*	↑ 0.27±0.4835	0.6213	↑0.21±0.2151	0.2943
miR-16	↑ 1.94±0.00	0.0005**	↓0.99±0.0318	<0.0001**	↑1.84±0.1487	0.0003**
miR-10b	↑ 2. 58±0.3490	0.0143*	↓ 1.185±0.3490	0.0290*	↑1.30±0.0263	0.0777
miR-152	↑ 2.59±0.1308	0.0094**	↓2.77±0.4653	0.0211*	↑0.77±0.3965	0.2270
Let-7f	↑ 4.40±0.2102	<0.0001**	↑0.11±0.0082	0.4869	↑1.8±0.0510	<0.0001**

Unpaired *t* test P_{value}<0.05*; P_{value}<0.01**; NED, no expression detected following tumor challenge.

Table S4 Tumor Vasculature cf Normal Vasculature.

miR	NV†	TV‡	Fold	*miR*	NV	TV	Fold	*miR*	NV	TV	Fold	*miR*	NV	TV	Fold
miR-451	14955.10	298.31	↓50.13	**Let-7i**	2960.39	1401.32	↓2.11	**miR-155**	805.29	631.46	↓1.28	**miR-130b**	163.41	291.84	↑1.79
miR-486	93.75	1.90	↓49.24	**miR-30d**	15236.90	7551.81	↓2.02	**miR-28***	999.18	809.08	↓1.23	**miR-872***	74.02	133.64	↑1.81
miR-128	1911.53	104.32	↓18.32	**miR-140***	16011.70	7984.72	↓2.01	**miR-146a**	2035.75	1665.55	↓1.22	**miR-27a***	233.59	422.43	↑1.81
miR-181a-1*	238.97	20.94	↓11.41	**miR-1944**	271.76	140.49	↓1.93	**miR-532-5p**	239.74	199.89	↓1.20	**miR-379**	99.12	182.57	↑1.84
miR-181b	11996.30	1100.72	↓10.90	**miR-26b**	1431.28	740.54	↓1.93	**miR-378**	36453.00	31532.20	↓1.16	**miR-301b**	39.70	84.91	↑2.14
miR-181a	52139.40	5188.74	↓10.05	**miR-200b**	73.77	38.45	↓1.92	**miR-15b***	50.46	44.17	↓1.14	**miR-320**	40.98	88.52	↑2.16
miR-30a	7154.58	846.58	↓8.45	**miR-15a**	439.27	229.40	↓1.91	**miR-125a-5p**	572.72	509.43	↓1.12	**miR-23a**	1056.55	2352.98	↑2.23
miR-30a*	970.75	146.40	↓6.63	**miR-10a**	9726.68	5113.36	↓1.90	**miR-223**	978.43	876.66	↓1.12	**miR-9**	62.24	144.49	↑2.32
miR-150*	137.54	21.51	↓6.39	**miR-339-3p**	77.61	40.93	↓1.90	**miR-103**	6674.33	6026.37	↓1.11	**miR-221**	186.72	437.09	↑2.34
miR-20b	648.28	113.46	↓5.71	**miR-98**	401.62	216.26	↓1.86	**miR-425**	948.21	868.66	↓1.09	**miR-27b***	30.74	72.91	↑2.37
miR-150	6572.65	1245.21	↓5.28	**miR-744**	1012.75	560.45	↓1.81	**Let-7d***	133.96	123.93	↓1.08	**miR-152**	282.77	679.43	↑2.40
miR-363	58.14	11.80	↓4.93	**miR-26a**	11246.30	6339.15	↓1.77	**miR-652**	189.80	180.28	↓1.05	**miR-542-3p**	30.99	75.39	↑2.43
miR-181d	634.19	129.07	↓4.91	**miR-342-5p**	123.20	71.39	↓1.73	**miR-143**	8326.40	8093.61	↓1.03	**miR-182**	604.48	1483.56	↑2.45
miR-194	581.94	125.45	↓4.64	**miR-20a**	1136.21	658.49	↓1.73	**miR-191**	6521.93	6349.62	↓1.03	**miR-362-5p**	30.48	82.43	↑2.70
miR-200c	751.50	167.91	↓4.48	**miR-140**	460.53	268.42	↓1.72	**miR-17**	561.19	549.60	↓1.02	**miR-21**	32453.70	88627.30	↑2.73
miR-126-5p	662.36	159.91	↓4.14	**Let-7a**	70562.50	41335.90	↓1.71	**miR-374**	197.48	195.51	↓1.01	**miR-151-3p**	515.85	1539.34	↑2.98
miR-126-3p	8108.17	2099.41	↓3.86	**miR-142-5p**	2650.73	1606.54	↓1.65	**miR-101b**	850.88	890.74	↑1.05	**miR-99b**	2154.08	6693.24	↑3.11
miR-142-3p	32310.50	8430.57	↓3.83	**miR-148a**	3294.39	2007.08	↓1.64	**miR-1839-5p**	306.34	320.78	↑1.05	**miR-351**	18.70	58.25	↑3.12
miR-106b*	201.32	54.07	↓3.72	**miR-1**	506.63	310.30	↓1.63	**miR-145**	96.56	101.28	↑1.05	**miR-183**	199.78	696.76	↑3.49
miR-1198	64.03	17.51	↓3.66	**miR-532-3p**	50.71	31.98	↓1.59	**miR-22**	418.52	462.03	↑1.10	**miR-7a**	663.13	2456.54	↑3.70
miR-186	2056.24	638.88	↓3.22	**Let-7g**	16711.40	10546.20	↓1.58	**miR-24-2***	149.33	167.72	↑1.12	**miR-222**	76.33	329.15	↑4.31
miR-106b	1133.90	353.71	↓3.21	**miR-203**	150.86	96.52	↓1.56	**miR-423-5p**	604.22	720.36	↑1.19	**miR-132**	49.18	214.36	↑4.36
miR-25	2960.65	937.77	↓3.16	**miR-16**	10760.20	7201.91	↓1.49	**miR-149**	111.42	132.88	↑1.19	**miR-100**	163.93	715.98	↑4.37
miR-106a	127.30	41.31	↓3.08	**miR-34c**	159.83	108.89	↓1.47	**miR-27b**	958.45	1161.45	↑1.21	**Let-7e**	177.25	954.90	↑5.39
miR-99a	99.38	32.74	↓3.04	**Let-7f**	114408.00	78289.00	↓1.46	**miR-322**	266.12	327.06	↑1.23	**miR-125b-5p**	576.05	3442.66	↑5.98
miR-29a	5195.93	1722.66	↓3.02	**miR-18a**	123.97	86.24	↓1.44	**miR-24**	23722.10	29541.00	↑1.25	**miR-210**	4.61	50.07	↑10.86
miR-342-3p	1515.80	523.71	↓2.89	**Let-7b**	4913.41	3421.15	↓1.44	**miR-1981**	330.41	429.10	↑1.30	**miR-503**	6.40	71.20	↑11.12
miR-30e*	2370.52	832.11	↓2.85	**miR-484**	130.12	90.62	↓1.44	**miR-365**	54.30	73.48	↑1.35	**miR-130a**	11.78	180.47	↑15.32
miR-30e	5810.14	2047.82	↓2.84	**Let-7d**	2464.78	1719.24	↓1.43	**miR-127**	115.00	157.44	↑1.37	**miR-199a-5p**	13.83	213.22	↑15.42
miR-30c	8512.35	3042.12	↓2.80	**miR-15b**	1193.07	833.44	↓1.43	**miR-148b**	956.92	1318.89	↑1.38	**miR-129-5p**	5.12	84.52	↑16.50
miR-93	7240.13	2622.55	↓2.76	**miR-30b**	560.93	392.35	↓1.43	**miR-151-5p**	113.72	161.82	↑1.42	**miR-31**	12.81	285.94	↑22.33
miR-192	527.12	204.08	↓2.58	**miR-29b**	76.84	54.83	↓1.40	**miR-2133**	249.99	357.14	↑1.43	**miR-196b**	43.80	1217.61	↑27.80
miR-92a	5610.35	2238.19	↓2.51	**miR-19b**	164.95	120.31	↓1.37	**miR-27a**	834.74	1206.38	↑1.45	**miR-214**	3.84	122.22	↑31.81
miR-139-5p	457.97	183.33	↓2.50	**miR-185**	52.00	38.07	↓1.37	**miR-872**	351.67	522.38	↑1.49	**miR-125b-3p**	2.05	73.48	↑35.86
miR-29c	58.40	25.51	↓2.29	**miR-101a**	407.51	306.69	↓1.33	**miR-23b**	331.44	503.53	↑1.52	**miR-10b**	37.40	3879.75	↑103.75
miR-181c	237.69	106.80	↓2.23	**Let-7c**	50555.90	38120.20	↓1.33	**miR-340-5p**	131.14	211.69	↑1.61				
miR-423-3p	356.03	160.86	↓2.21	**miR-361**	117.82	90.62	↓1.30	**miR-28**	145.74	246.91	↑1.69				
miR-340-3p	70.18	31.98	↓2.19	**miR-195**	52.00	40.74	↓1.28	**miR-541**	60.45	103.56	↑1.71				

†NV, Normal Vasculature; ‡TV, Tumor Vasculature

Table S5A Tumor Vasculature cf Normal Vasculature (Log_2 Normalised Expression)

miRNA	Log_2Fold	Pri-miRNA	Log_2Fold
miR-451	↓5.65	miR-451	↓5.65
miR-30a	↓3.08	miR-30a	↓3.03
miR-151-3p	↑1.58	miR-151	↑1.43
miR-7a	↑1.89	miR-7a-1	↑1.87
-	-	miR-7a-2	↑1.90
miR-132	↑2.12	miR-132	↑2.08
miR-152	↑1.26	miR-152	↑1.26
miR-31	↑4.48	miR-31	↑4.50
miR-10b	↑6.70	miR-10b	↑6.70

Pri vs mature levels r^2 =0.9998, by Pearsons correlation

Table S5B Tumor Vasculature cf Normal Vasculature (Log_2 Normalised Expression)

	LLC		MDA-MB-231		4T1	
	Log_2Fold	P_{value}	Log_2Fold	P_{value}	Log_2Fold	P_{value}
miR-451	↓4.80±0.54	<0.0001**	↓4.16±0.34	<0.0001**	↑1.16±0.21	0.0055**
miR-30a	↓1.4±0.20	0.0114*	↓1.13±0.21	0.0062**	↑1.79±0.23	0.0012**
miR-151-3p	↑2.34±0.61	0.0169*	↑1.36±0.12	0.0102*	↑4.66±0.21	<0.0001**
miR-7a	↑2.07±0.20	0.0084**	↑1.50±0.35	0.0100*	↓0.60±0.12	0.3297
miR-132	↑1.63±.09	0.0067**	↑1.51±0.0.12	0.0982	↑5.92±0.13	<0.0001**
miR-152	↑1.42±0.68	0.3064	↑1.91±0.44	0.0166*	↑4.30±0.9	<0.0001**
miR-31	↑2.52±0.34	0.0005**	↑4.23±0.12	<0.0001**	↑7.9±0.47	<0.0001**
miR-196b	↑4.37±0.55	0.0429*	↑3.00±0.42	0.0010*	↑6.75±0.30	<0.0001**
miR-10b	↑3.84±0.55	0.0016**	↑2.08±0.10	0.0015**	↑3.09±0.26	0.0022**

P_{value}<0.05*; P_{value}<0.01**; Unpaired *t* test

Table S5C Tumor Vasculature cf Normal Vasculature (Log_2 Normalised Expression), following cherry exclusion.

	No Exclusion		Cherry Exclusion	
	Log_2Fold	P_{value}	Log_2Fold	P_{value}
miR-10b	↑3.84±0.54	0.0016**	↑5.07±0.48	<0.0001**
miR-132	↑1.63±0.09	0.0067**	↑1.01±0.27	0.0267*
miR-151-3p	↑2.34±0.61	0.0169*	↑1.14±0.19	0.0049**
miR-152	↑1.42±0.68	0.3064	↑1.38±0.60	0.0119*
miR-196b	↑4.37±0.53	0.0429*	↑4.35±0.47	0.0444*
miR-31	↑2.52±0.34	0.0005**	↑4.85±0.14	<0.0001**
miR-30a	↓1.40±0.20	0.0114*	↓3.56±1.09	0.0021**
miR-451	↓4.80±0.58	<0.0001**	↓5.87±0.39	<0.0001**
miR-7a	↑2.07±0.20	0.0084**	↓1.04±1.20	0.1676

P_{value}<0.05*; P_{value}<0.01**; Unpaired *t* test

Table S6A Tumor-Conditioned Media Experiments- Mouse ECs Mature miRNA

	LLC		4T1		MDA-MB-231	
	Log_2Fold	**P_{value}**	**Log_2Fold**	**P_{value}**	**Log_2Fold**	**P_{value}**
miR-196b	↑1.84±0.34	0.0082**	↑3.14±0.30	0.0004**	↑1.42±0.21	0.0045*
miR-10b	↑1.09±0.11	0.0004**	↑0.74±0.23	0.0426*	↑0.98±0.13	0.0015**
miR-152	↑0.37±0.24	0.1880	↑0.90±0.16	0.0018**	↓0.52±0.19	0.0347*
miR-7a	↑0.29±0.27	0.3383	↑0.57±0.15	0.0088**	↑0.35±0.13	0.0397*
miR-132	↑0.26±0.14	0.4926	↑0.40±0.01	0.2513	↑0.35±0.28	0.4778
miR-30a	↑0.12±0.14	0.6392	↑1.18±0.17	0.0044*	↓0.71±0.22	0.0540
miR-151-3p	↑0.08±0.20	0.7633	↑1.39±0.24	0.0024**	↑0.31±0.11	0.1266
miR-31	↓0.04±0.08	0.8053	↑0.04±0.14	0.9056	↓0.12±0.14	0.5382
miR-451	↓0.55±0.34	0.2936	↓1.32±0.31	0.0469*	↓0.98±0.16	0.0462*

P_{value}<0.05*; P_{value}<0.01**; Unpaired *t* test

Table S6B VEGF Induction in Mouse ECs

	6h		48h	
	Log_2Fold	**P_{value}**	**Log_2Fold**	**P_{value}**
miR-10b	↑0.66±0.05	0.0005**	↑1.33±0.17	0.0016**
miR-132	↑1.26±0.05	0.0140*	↑0.16±0.18	0.6909

P_{value}<0.05*; P_{value}<0.01**; Unpaired *t* test

Table S7A Human Tumor Vessels/Field

	IDC Grade III			DCIS		
	Median +ve	**Median -ve**	P_{value}	**Median +ve**	**Median -ve**	P_{value}
miR-10b	2.5	0	$P<0.0001$	0	3.5	$P<0.0001$
miR-196b	2	2	P=0.2389	0	4	$P<0.0001$

$P_{value}<0.05$*; $P_{value}<0.01$**; Mann Whitney U.

Table S7B VEGF Induction of Human ECs

	12h		***24h***	
	Log_2Fold	P_{value}	**Log_2Fold**	P_{value}
miR-196b	↑0.93±0.09	0.0023**	↑1.86±0.12	0.0003**
miR-132	↑1.25±0.09	0.0071**	↑1.58±0.10	0.0008**
miR-152	↑1.15±0.05	0.0002**	↑1.61±0.05	0.0025**
miR-10b	↑1.43±0.04	0.0019**	↑1.44±0.03	0.0005**
miR-31	↑0.31±0.07	0.0754	↑1.13±0.03	0.0001**

$P_{value}<0.05$*; $P_{value}<0.01$**; Unpaired t *t*est

Table S7C Tumor-Conditioned Media Induction of Human Cell Lines

	LLC		**MDA-MB-231**		**4T1**	
	Log_2Fold	P_{value}	**Log_2Fold**	P_{value}	**Log_2Fold**	P_{value}
miR-10b	↑0.58±0.05	0.01744**	↑0.68±0.05	0.0237*	↑0.37±0.07	0.6039

$P_{value}<0.05$*; $P_{value}<0.01$**; Unpaired *t* test

Table S8A Tube Number and Length Mouse ECs: anti-miR-10b

	16h		*18h*		*20h*		*22h*		*24h*		*26h*	
Tube Number	**No**	P_{value}	**No**	P_{value}	**No**	P_{value}	**No**	P_{value}	**No**	P_{value}	**No**	P_{value}
Anti-miR-10b	27.33±1.20	-	38.67±0.88	-	40.33±2.03	-	46.67±0.67	-	52.67±1.20	-	70.33±1.20	-
Transfect control	48.00±1.15	0.0002**	48.67±0.33	0.0004**	52.33±2.33	0.0178*	63.33±0.33	<0.0001**	73.33±3.18	0.0037**	85.67±0.67	0.0004**
Scrambled control	46.67±1.86	0.0009**	49.33±0.67	0.0006**	50.67±1.20	0.0118*	64.33±0.67	<0.0001**	75.00±2.65	0.0015**	88.33±2.40	0.0026**
Tube Length	**µM**	P_{value}	**µM**	P_{value}	**µM**	P_{value}	**µM**	P_{value}	**µM**	P_{value}	**µM**	P_{value}
Anti-miR 10b	112.48±2.01	-	128.50±1.93	-	133.88±0.37	-	134.77±0.68	-	140.70±0.35	-	143.33±1.15	-
Transfect control	141.53±1.67	0.0004**	143.50±1.38	0.0032**	146.78±2.69	0.0089**	163.12±0.90	<0.0001**	175.50±0.86	<0.0001**	176.87±1.39	<0.0001**
Scrambled control	144.40±0.23	<0.0001**	142.77±0.11	0.0018**	149.68±2.43	0.0030**	160.90±1.55	0.0001**	172.55±1.00	<0.0001**	173.48±1.89	0.0002**

Table S8B Tube Number and Length Human ECs: anti-miR-10b

	12h		*18h*		*24h*	
Tube Length	**µM**	P_{value}	**µM**	P_{value}	**µM**	P_{value}
Anti-miR 10b	64.33±1.45	-	61.33±1.45	-	58.00±1.73	-
Transfect control	80.67±0.33	0.0004**	75.67±2.91	0.0116*	75.67±1.76	0.0020**
Scrambled control	83.33±1.45	0.0008**	74.33±0.33	0.0010**	75.67±3.28	0.0089i*
Tube Number	**No**	P_{value}	**No**	P_{value}	**No**	P_{value}
Anti-miR 10b	124.07±3.33	-	137.68±1.51	-	133.83±0.85	-
Transfect control	168.10±4.39	0.0013**	171.60±1.58	0.0001**	199.78±0.43	<0.0001**
Scrambled control	164.55±3.56	0.0011**	173.78±3.00	0.0004**	199.25±0.35	<0.0001**

Table S8C Tube Number and Length Mouse ECs: anti-miR-196b

	16h		*18h*		*20h*		*22h*		*24h*		*26h*	
Tube Length	**µM**	P_{value}	**µM**	P_{value}	**µM**	P_{value}	**µM**	P_{value}	**µM**	P_{value}	**µM**	P_{value}
Anti-miR 196b	129.43±0.57	-	131.45±1.39	-	142.22±1.51	-	165.67±1.38	-	155.25±0.40	-	162.32±2.01	
Transfect control	157.53±0.79	<0.0001**	159.27±1.54	0.0002**	161.37±1.31	0.0007**	165.67±1.38	1.0000	168.08±1.25	0.0006**	170.52±0.79	0.0192*
Scrambled control	154.48±0.67	<0.0001**	157.45±1.34	0.0002**	158.75±1.95	0.0026**	164.97±2.76	0.8319	170.05±2.96	0.0077**	173.52±1.07	0.0079**
Tube Number	**No**	P_{value}	**No**	P_{value}	**No**	P_{value}	**No**	P_{value}	**No**	P_{value}	**No**	P_{value}
Anti-miR-196b	62.33±0.88	-	66.33±1.20	-	70.00±1.15	-	73.00±1.15	-	75.67±1.20	-	80.33±2.19	-
Transfect control	74.00±0.00	0.0002**	78.00±0.58	0.0009**	82.67±0.88	0.0010**	85.67±0.88	0.0010**	87.67±1.76	0.0049**	90.33±2.40	0.0370*
Scrambled control	77.00±2.65	0.0063**	80.67±0.88	0.0007**	83.67±0.33	0.0003**	87.33±0.67	0.0004**	89.00±1.73	0.0032**	91.33±0.88	0.0095**

Table S8D Tube Number and Length Human ECs: anti-miR-196b

	12h		*18h*		*24h*	
Tube Length	**µM**	P_{value}	**µM**	P_{value}	**µM**	P_{value}
Anti-miR 196b	55.00±2.89	-	63.00±4.73	-	54.00±5.86	-
Transfect control	69.33±2.33	0.0181*	73.67±2.33	0.1130	64.67±3.84	0.2026
Scrambled control	67.00±0.58	0.0151*	70.00±0.00	0.2979	59.67±1.76	0.4068
Tube Number	**No**	P_{value}	**No**	P_{value}	**No**	P_{value}
Anti-miR 196b	141.78±4.52	-	145.43±3.21	-	148.72±2.95	-
Transfect control	155.73±0.67	0.0388*	176.43±1.63	0.0010**	190.93±3.90	0.0010**
Scrambled control	161.33±3.40	0.0259*	172.40±5.60	0.0139*	191.92±7.79	0.0066**

Table S8E Wound Healing Assay Mouse ECs: anti-miR-10b

	6h		*8h*		*10h*		*12h*	
	%Migration	P_{value}	**%Migration**	P_{value}	**%Migration**	P_{value}	**%Migration**	P_{value}
Anti-miR 10b	9.14±1.26	-	15.79±1.05	-	15.95±1.34	-	20.42±1.61	-
Transfect control	9.32±1.08	0.9203	33.15±1.05	0.0003**	44.73±1.21	<0.0001**	50.02±0.98	<0.0001**
Scrambled control	9.10±1.61	0.9829	34.24±0.78	0.0001**	44.66±0.59	<0.0001**	48.74±1.29	<0.0001**

Table S8F Wound Healing Human ECs: anti-miR-10b

	2h		*4h*		*6h*		*8h*	
	%Migration	P_{value}	**%Migration**	P_{value}	**%Migration**	P_{value}	**%Migration**	P_{value}
Anti-miR 10b	8.31±1.32	-	13.86±0.99	-	24.42±1.64	-	31.11±0.80	-
Transfect control	9.03±0.83	0.6695	21.34±1.44	0.0128**	32.98±1.51	0.0185*	60.28±1.22	<0.0001**
Scrambled control	8.01±0.68	0.8485	19.82±0.86	0.0104**	32.60±1.07	0.0140**	58.40±1.07	<0.0001**

Table S8G Wound Healing Mouse ECs: anti-miR-196b

	6h		*8h*		*10h*		*12h*	
	%Migration	P_{value}	**%Migration**	P_{value}	**%Migration**	P_{value}	**%Migration**	P_{value}
Anti-miR-196b	5.08±0.77	-	6.05±1.34	-	16.85±0.41	-	20.50±1.51	-
Transfect control	6.38±0.56	0.2425	19.76±0.49	0.0006**	33.63±1.46	0.0004**	45.24±0.30	<0.0001**
Scrambled control	3.16±0.28	0.0783	21.27±1.27	0.0012**	34.70±0.88	<0.0001**	44.43±2.50	<0.0001**

Table S8H Wound Healing Human ECs: anti-miR-196b

	2h		*4h*		*6h*		*8h*	
	%Migration	P_{value}	**%Migration**	P_{value}	**%Migration**	P_{value}	**%Migration**	P_{value}
Anti-miR-196b	7.80±1.32	-	11.87±0.23	-	15.93±0.08	-	22.37±0.91	-
Transfect control	7.99±1.02	0.9134	18.70±0.57	0.0004**	23.37±0.81	0.0008**	56.34±0.97	<0.0001**
Scrambled control	7.34±1.34	0.8177	21.02±0.89	0.0006**	26.39±0.29	<0.0001**	58.09±1.18	<0.0001**